



Stephan Pranter BSc

# **Active Noise Cancellation (ANC) Concept Development**

## **MASTER'S THESIS**

to achieve the university degree of  
Master of Science

Master's degree programme: Electrical Engineering

submitted to

**Graz University of Technology**

Supervisor

Ass.Prof. Dipl.-Ing. Dr.techn. Peter Söser

Institute of Electronics

Advisor

Johnny Pedersen, MSc, MBA - USound GmbH

Graz, March 2021

## **AFFIDAVIT**

I declare that I have authored this thesis independently, that I have not used other than the declared sources/resources, and that I have explicitly indicated all material which has been quoted either literally or by content from the sources used. The text document uploaded to TUGRAZonline is identical to the present master's thesis dissertation.

---

Date

---

Signature

## Kurzfassung

Kopfhörer mit aktiver Geräuschunterdrückung (ANC) haben sich in den letzten Jahren im professionellen sowie im kommerziellen Bereich etabliert. Der aktuelle Trend im Kopfhörermarkt geht in Richtung True Wireless Stereo Ohrhörer mit inkludierter aktiver Geräuschunterdrückung. Kapazitive MEMS Lautsprecher bieten sich aufgrund ihrer kleinen Bauform und ihrer hohen Audioqualität für diese Art der Anwendung an. Diese Diplomarbeit beschäftigt sich daher mit der Entwicklung eines ANC-Technologiedemonstrators für MEMS Lautsprecher. Der Demonstrator basiert auf speziellen, im 3D-Druckverfahren hergestellten Ohrhörern, und einem kommerziell verfügbaren analogen ANC Baustein. Ausgehend von den Charakterisierungsmessungen an den Ohrhörern werden die analogen Filter entworfen und implementiert. Anschließend wird die erreichte Geräuschunterdrückung des Demonstrators gemessen, sowie der Einfluss verschiedener Mikrofone verglichen. Abschließend wird ein Ausblick auf die zukünftige Arbeit am Demonstrator gegeben.

## **Abstract**

Headphones with active noise cancellation (ANC) have become well established in both professional and commercial fields in the last years. The recent trend is towards true wireless stereo earphones with included active noise cancellation functionality. Due to their small size and high audio performance, capacitive MEMS speakers are attractive candidates for these type of applications. Therefore, this work is concerned with the development of an active noise cancellation demonstrator which utilizes USound MEMS speakers. The demonstrator is based on 3d printed in-ear headphone prototypes and a commercially available analog active noise cancelling IC solution. After characterization measurements on the earphones, the appropriate analog noise cancellation filters are designed and implemented. The performance of the demonstrator is then measured and analyzed also with respect to the used microphone types. Finally, an outlook on future work is given.

# Contents

<b>1</b>	<b>Introduction</b>	<b>1</b>
1.1	Background . . . . .	1
1.1.1	History . . . . .	1
1.2	Fields of Application . . . . .	2
1.2.1	Basic Mechanism . . . . .	3
1.3	Aim and Scope . . . . .	4
1.4	Thesis Outline . . . . .	4
<b>2</b>	<b>Basics</b>	<b>5</b>
2.1	Important Definitions . . . . .	5
2.1.1	The Decibel - dB . . . . .	5
2.1.2	Sound Pressure Level - SPL . . . . .	6
2.1.3	Total Harmonic Distortion - THD . . . . .	6
2.1.4	Signal to Noise Ratio - SNR . . . . .	7
2.2	The Measurement System . . . . .	7
2.2.1	Audio Precision APx525 . . . . .	7
2.2.2	APx1701 Transducer Test Interface . . . . .	7
2.2.3	Ear Simulator . . . . .	7
2.3	Microphones . . . . .	8
2.3.1	Electret Condenser Microphones . . . . .	8
2.3.2	MEMS Microphones . . . . .	10
2.3.3	Important Properties for ANC . . . . .	11
2.3.4	Comparison . . . . .	12
2.4	Analog Filters . . . . .	13
2.4.1	High Pass Filter . . . . .	13
2.4.2	Low Pass Filter . . . . .	14
2.4.3	Shelving Filters . . . . .	15
2.4.4	Notch Filter . . . . .	17
2.5	MEMS Speaker . . . . .	18
<b>3</b>	<b>Active Noise Cancellation</b>	<b>20</b>
3.1	ANC Topologies . . . . .	20
3.1.1	Feedforward . . . . .	20
3.1.2	Feedback . . . . .	20
3.1.3	Hybrid . . . . .	21

3.2	Analog versus Digital ANC Systems . . . . .	22
3.2.1	Analog Systems . . . . .	22
3.2.2	Digital Systems . . . . .	22
3.2.3	Comparison . . . . .	27
3.3	ANC Headphones on the Market . . . . .	27
3.3.1	Over-the-Ear Headphones . . . . .	28
3.3.2	In-Ear Headphones . . . . .	28
3.3.3	Summary . . . . .	30
<b>4</b>	<b>Development of ANC Demonstrator</b>	<b>31</b>
4.1	Earphones . . . . .	31
4.2	MEMS Speaker Driver . . . . .	31
4.3	USound Ananke Board . . . . .	32
4.4	Noise Cancelling IC AS3435 . . . . .	33
4.5	The Proposed Concept . . . . .	35
4.5.1	Audio Signal Path . . . . .	35
4.6	Feedback System . . . . .	36
4.6.1	The Prototype . . . . .	36
4.6.2	Earphone Characterization . . . . .	37
4.6.3	Adjustments . . . . .	39
4.7	Feedforward System . . . . .	41
4.7.1	The Prototype . . . . .	41
4.7.2	Earphone Characterization . . . . .	41
4.7.3	Filter Design . . . . .	45
4.8	Implementation . . . . .	47
4.9	Measurement of Performance of the 1st FF System . . . . .	48
4.9.1	Feedforward System Left Channel . . . . .	48
4.9.2	Feedforward System Right Channel . . . . .	49
4.9.3	Adjustments . . . . .	50
4.10	Recharacterization and Redesign . . . . .	52
4.10.1	Left Channel - MEMS Microphone . . . . .	52
4.10.2	Right Channel - Electret Microphone . . . . .	53
4.11	Measurement of Performance of the 2nd FF System . . . . .	55
4.12	Subjective Evaluation . . . . .	55
4.13	Effect of Leakage . . . . .	56
4.13.1	MEMS Speaker Response . . . . .	56
4.13.2	Passive Attenuation . . . . .	56
4.13.3	ANC Performance . . . . .	57
<b>5</b>	<b>Results and Discussion</b>	<b>59</b>
5.1	Feedback System . . . . .	59
5.2	Feedforward System . . . . .	59
<b>6</b>	<b>Closure</b>	<b>61</b>
6.1	Conclusions . . . . .	61
6.1.1	Improvements . . . . .	61

6.2 Future Work . . . . .	62
<b>7 Appendix</b>	<b>63</b>

# List of Figures

1.1	First description of feedforward and feedback ANC systems . . . . .	2
1.2	Active noise cancellation in a headphone . . . . .	3
2.1	Acoustic spectrum of a headphone-speaker-signal when excited with a 1 kHz sinus tone, taken from [1] . . . . .	6
2.2	GRAS RA0045 Externally Polarized Ear Simulator . . . . .	8
2.3	Cross section of an electret condenser microphone according to [2] . . . . .	9
2.4	Commonly used preamplifier circuit for electret condenser microphones . . . . .	9
2.5	Cross section of a MEMS transducer according to [3] . . . . .	10
2.6	MEMS microphone types according to [4] . . . . .	11
2.7	Example microphone phase and magnitude response according to [5] . . . . .	11
2.8	Determination of the dynamic range of a microphone according to [3] . . . . .	12
2.9	Passive high pass filter . . . . .	13
2.10	Passive low pass filter . . . . .	14
2.11	Lossy integrator as active low-pass filter . . . . .	15
2.12	Active high shelf filter . . . . .	16
2.13	Active low shelf filter . . . . .	17
2.14	Schematic of a notch filter . . . . .	18
2.15	Frequency response of the notch filter for different values of $R_d$ . . . . .	18
2.16	Bending of a piezoelectric cantilever due to an applied voltage, taken from [6] . . . . .	18
2.17	MEMS motor consisting of multiple cantilevers, taken from [6] . . . . .	19
2.18	Membrane attached to MEMS motor to generate sound, taken from [6] . . . . .	19
2.19	Electro-mechanical-acoustical spice model of a MEMS speaker . . . . .	19
3.1	Feedforward and feedback ANC topologies . . . . .	21
3.2	Hybrid ANC topology . . . . .	21
3.3	Block diagram of an analog feedforward ANC system . . . . .	22
3.4	Digital feedforward system for noise control in a duct . . . . .	23
3.5	FIR filter structure . . . . .	23
3.6	IIR filter structure . . . . .	24
3.7	Typical adaptive filter . . . . .	24
3.8	Digital feedforward system using the FXLMS algorithm for noise control in a duct . . . . .	27
4.1	Megaclite USB-C headset . . . . .	31
4.2	LM48560 speaker driver IC with necessary passive components . . . . .	32

4.3	Block diagram of the Ananke evaluation board . . . . .	33
4.4	AS3435 Block diagram taken from the datasheet [7] . . . . .	34
4.5	Option 1: routing audio through the AS3435 . . . . .	35
4.6	Option 2: routing audio directly to the LM48560 . . . . .	36
4.7	Impact of AS3435 noise cancelling IC on audio performance. Measured LM48560 output voltage with 22 nF capacitor as load for speaker voltages of 1.1 V <sub>rms</sub> and 9 V <sub>rms</sub> . . . . .	37
4.8	Feedback ANC prototype earphone . . . . .	38
4.9	Measurement setup for the characterization of the feedback system . . . . .	39
4.10	Characterization measurement results for the feedback system with SPH1642 MEMS microphone . . . . .	39
4.11	Deviation of the magnitude response of the FB microphones from the magnitude response of the acoustic coupler . . . . .	40
4.12	Change in magnitude response when increasing the vent diameter . . . . .	40
4.13	Change in magnitude response when the ear canal is blocked . . . . .	41
4.14	Characterization of a FF ANC system . . . . .	42
4.15	SPL measurement in the near field of the loudspeakers . . . . .	43
4.16	Measurement setups for characterization measurements 1 and 2 . . . . .	44
4.17	Measurements are performed in the near field of electrodynamic speakers . . . . .	44
4.18	Measurement setup for characterization measurement 3 . . . . .	45
4.19	Frequency response of designed filter versus target filter for the left channel . . . . .	46
4.20	Filter for left channel using a MEMS microphone for ANC . . . . .	46
4.21	Frequency response of designed filter versus ideal filter . . . . .	47
4.22	Filter for right channel using an ECM microphone for ANC . . . . .	48
4.23	AS3435 evaluation board with ANC filters for the feedforward prototype . . . . .	48
4.24	Block diagram for ANC performance measurements . . . . .	49
4.25	Measured ANC performance of left channel at 110 dB SPL . . . . .	49
4.26	Measured ANC performance of right channel at 110 dB SPL . . . . .	50
4.27	Different types of eartips that have been investigated. From left to right: black, red, transparent black . . . . .	50
4.28	Passive attenuation measurement results . . . . .	51
4.29	Frequency response of previously designed filter versus ideal filter after recharacterization . . . . .	51
4.30	Prototype earphone used for the recharacterization measurements . . . . .	52
4.31	Frequency response of designed filter versus ideal filter - MEMS microphone . . . . .	53
4.32	Schematic of the redesigned ANC filter with MEMS feedforward microphone . . . . .	53
4.33	Frequency response of designed filter versus ideal filter - electret microphone . . . . .	54
4.34	Schematic of the redesigned ANC filter - electret microphone . . . . .	54
4.35	Passive attenuation vs active attenuation of the recharacterized system at 106 dB SPL . . . . .	55
4.36	Leakage is simulated by placing wire between coupler and eartip . . . . .	56
4.37	Loss of bass response with increased leakage . . . . .	57
4.38	Reduction in passive attenuation due to increased leakage . . . . .	58
4.39	Reduction in ANC performance due to increased leakage . . . . .	58
5.1	ANC performance at 106 dB SPL . . . . .	60

# List of Tables

2.1	Comparison of MEMS and electret microphones for ANC applications . . .	13
3.1	Comparison of analog and digital ANC systems . . . . .	27
3.2	Available wired over-the-ear ANC headphones . . . . .	28
3.3	Available wireless over-the-ear ANC headphones . . . . .	29
3.4	Available wired in-ear ANC headphones . . . . .	29
3.5	Available wireless in-ear ANC headphones . . . . .	30
4.1	Comparison of available noise cancelling ICs . . . . .	33
7.1	Electret microphones for ANC . . . . .	64
7.2	MEMS microphones for ANC . . . . .	64

# Chapter 1

## Introduction

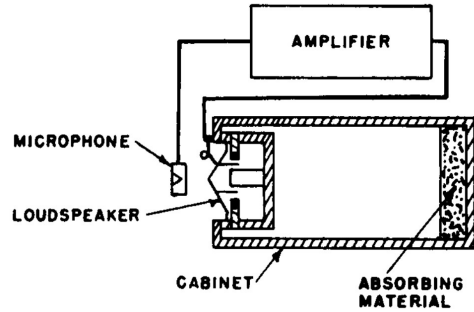
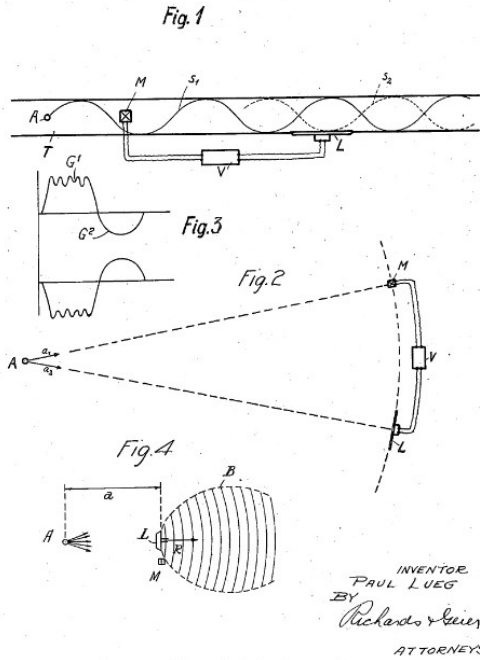
### 1.1 Background

In today's world an ever increasing amount of people are constantly surrounded by noise. Traffic, industrial sounds or household sounds are just a few of the ubiquitous sources in everyday life. Therefore, the idea of reducing the noise exposure to the individual by technical means is rather popular. This is where active noise cancellation (ANC) comes into play. This technology is based on destructive interference of noise with generated anti-noise to reduce the overall noise perceived by the user. ANC can also be used to enhance the listening experience when using headphones by suppressing undesired disturbances from the outside world and this is the main motivation for this work.

#### 1.1.1 History

The beginnings of active noise cancellation go back to the early 1930s when the first patents on the topic were filed by Henri Coanda. Although his concept was technically flawed, he was the first one to describe destructive interference with anti phase sound [8]. Shortly after Coanda, the patents of the German scientist Paul Lueg followed. Lueg correctly described a method of sound cancellation by superposition of the original noise signal with an out of phase version of that signal so that the two would cancel each other out [9]. Figure 1.1a shows the original drawings of said patent. The figures show a feedforward system consisting of a microphone and a loudspeaker to reduce the noise in a duct as well as the principle of spacial noise reduction.

Both Coanda and Lueg could not demonstrate their ideas practically due to the technical limitations of the time. The first real demonstrators of active noise cancellations only came up in the 1950s when Olson and May presented an electronic sound absorber [10]. It consisted of a microphone that was mounted directly in front of a loudspeaker to reduce the sound pressure in the vicinity of the microphone. Figure 1.1b shows the block diagram of this feedback system.



(b) Elements of the electronic sound absorber according to [10]

(a) Original drawings taken from Lueg's patent [9]

Figure 1.1: First description of feedforward and feedback ANC systems

In 1955, Conover presented an application for actively reducing the noise of large transformers [11]. The system had multiple channels, one to cancel out the fundamental frequency of the humming noise of the transformer and two more channels to cancel the first two harmonics. For each of these channels the phase and amplitude had to be manually adjusted, and therefore, the system was only of little practical importance.

The next big steps were made in the 1980s when Chaplin and Smith announced a waveform synthesis technique and Burgess presented a broad band noise cancellation system using adaptive filters. [12]

Although the first ideas about active earmuffs date back to the 1950s, it was only in 1986 when the first wearable prototypes were created. Three years later, in 1989, the first commercially available ANC headset was introduced to the market by Bose [13].

## 1.2 Fields of Application

Today the ANC technology is successfully used in a variety of fields:

- **Headphones:** Commercial over-the-ear, in-ear and on-ear headphones with ANC functionality are widely available these days. Performance benchmarks on some available devices are reported in [14].

- Ventilation ducts: The use of ANC in ducts following Lueg's initial idea is widely established [13].
- Vehicle interiors: Commercial applications in cabins of propeller aircraft e.g. the SAAB2000 and cars [13].
- Open spaces: Applications with ANC for reducing transformer noise are reported in [15]

It is to be expected that, while the technology is being improved further and the system costs go down, more and more commercial applications will become possible. Promising fields are:

- Household appliances: Studies indicate the feasibility of active noise control in household appliances. For example, a washing machine was modified with vibration actuators and an average of 7 dB in noise reduction was reported [16].
- Smart materials: First studies with so called smart foams have been conducted. It has been shown that the attenuation properties of passive foam can be increased by the use of an embedded distributed piezoelectric actuator [17]

### 1.2.1 Basic Mechanism

The basic idea of active noise cancellation can best be explained with the aid of figure 1.2. The scenario is an over-the-ear headphone with ANC in a noisy environment. In order to cancel out unwanted signals, the noise (red curve) is recorded and an inverted version of this noise is created by the internal ANC system. This inverted noise signal (black curve) is played back via the headphones. At the human ear, both the noise and inverted noise arrive at the same time and therefore cancel each other out by destructive interference. In an ideal world, this would result in a perfect cancellation, in reality, however, there is always some residual noise left (green curve).

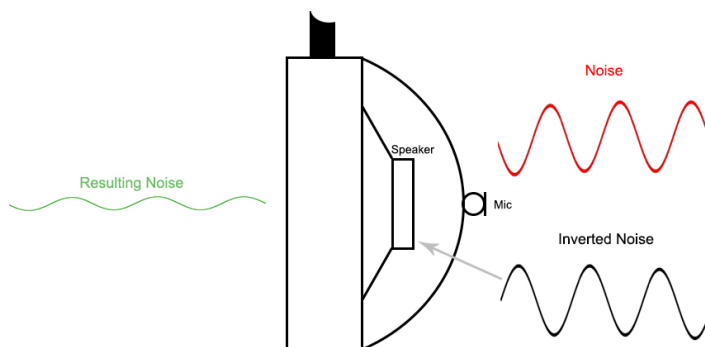


Figure 1.2: Active noise cancellation in a headphone

### 1.3 Aim and Scope

The aim of this thesis is to acquire knowledge in the field of ANC and use this knowledge to build a first technology demonstrator. This demonstrator will be based on an existing USound product with added active noise cancelling functionality. An analog off-the-shelf solution shall be used to implement the active noise cancellation functionality.

### 1.4 Thesis Outline

Chapter 1 served as a short introduction into the field of ANC and laid out the motivation for this thesis. In Chapter 2, the most important basics for this work will be discussed, whereas Chapter 3 gives a more detailed description of active noise cancellation. The development process for the technology demonstrator is documented in Chapter 4. The findings and results of this thesis are discussed in Chapter 5 and, finally, Chapter 6 draws a conclusion and gives some outlook on future work on this topic.

# Chapter 2

## Basics

### 2.1 Important Definitions

The most important quantities and definitions for this work are briefly described in this section.

#### 2.1.1 The Decibel - dB

The decibel (dB) is a logarithmic ratio of two numbers and is unitless. For power quantities, the calculation is done according to equation 2.1, where  $P_{ref}$  is a reference power. Depending on the choice of the reference, different dB notations are common, e.g., dBm is used for  $P_{ref} = 1 \text{ mW}$ .

$$L[dB] = 10 \cdot \log \left( \frac{P}{P_{ref}} \right) \quad (2.1)$$

When working with amplitude quantities, equation 2.1 can be rewritten to equation 2.2, where  $U_{ref}$  is a reference amplitude. In case of voltages a reference of  $U_{ref} = 1 \text{ V}$  is quite common and the resulting logarithmic ratio is then denoted by dBV.

$$L[dB] = 10 \cdot \log \left( \frac{U^2}{R} \cdot \frac{R}{U_{ref}^2} \right) = 20 \cdot \log \left( \frac{U}{U_{ref}} \right) \quad (2.2)$$

Since many quantities in acoustics have a large dynamic range, using the decibel allows for more handy numbers and a better comparability.

### 2.1.2 Sound Pressure Level - SPL

The Sound Pressure Level (SPL) is defined according to equation 2.3:

$$SPL[dB] = 20 \cdot \log\left(\frac{p}{p_0}\right) \quad (2.3)$$

where  $p$  is the actual sound pressure and  $p_0$  is the reference sound pressure of  $20 \mu Pa$ . The  $20 \mu Pa$  represent the average hearing threshold of humans for a frequency of 1 kHz. It is very common that certain characteristics of a microphone, for example, are specified for a 1 kHz sine wave at 94 dB SPL. According to equation 2.3, this point corresponds to a sound pressure of  $1 Pa$ .

### 2.1.3 Total Harmonic Distortion - THD

The total harmonic distortion (THD) is an important performance criterion for any audio system, since it gives information about the distortion introduced by the system. It is defined as the ratio of the RMS level of the generated harmonic frequencies  $k_i$  ( $i \geq 2$ ) to the RMS level of the fundamental  $k_1$ . Accordingly, the THD can be calculated with the aid of equation 2.4.

$$THD[\%] = \frac{\sqrt{\sum_{i=2}^{\infty} k_i^2}}{k_1} \quad (2.4)$$

Figure 2.1 shows an example spectrum for a speaker excited with a 1 kHz sine wave. The fundamental  $k_1$  is the tallest spike, the bins at 2 kHz ( $k_2$ ), 3 kHz ( $k_3$ ), 4 kHz ( $k_4$ ) etc., the harmonics generated by the speaker.

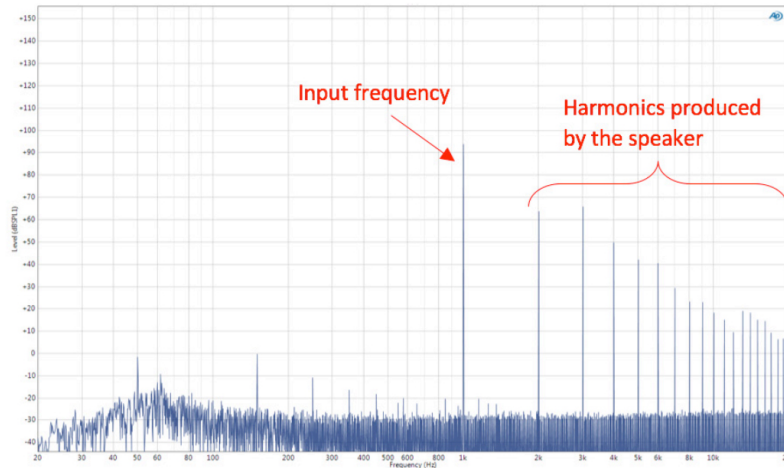


Figure 2.1: Acoustic spectrum of a headphone-speaker-signal when excited with a 1 kHz sinus tone, taken from [1]

A similar metric to THD is the THD+N, which also accounts for the noise in the system as indicated in equation 2.5.

$$THD + N[\%] = \frac{\sum_{i=2}^{\infty} \text{Harmonics} + \text{Noise}}{\text{Fundamental}} \quad (2.5)$$

Note that the statement of THD or THD+N alone is not sufficient. The corresponding measurement bandwidth (e.g. 20 Hz to 20 kHz), for example, has to be stated as well. The THD is frequency-dependent and therefore often specified via a measurement graph.

### 2.1.4 Signal to Noise Ratio - SNR

The signal to noise ratio (SNR) is a measure for signal quality and is defined according to equation 2.6, where  $P_S$  is the signal power and  $P_N$  is the noise power. Due to the large dynamic range, it is usually stated in decibels allowing for smaller numbers.

$$SNR[dB] = 10 \cdot \log \left( \frac{P_S}{P_N} \right) \quad (2.6)$$

## 2.2 The Measurement System

### 2.2.1 Audio Precision APx525

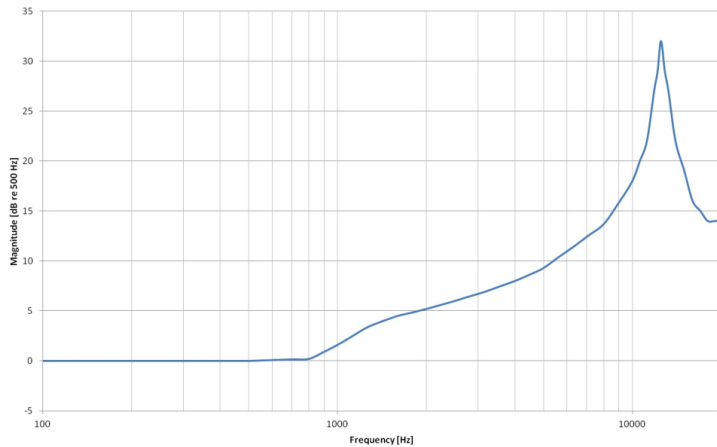
For this work, an Audio Precision APx525 audio analyzer was used. It features two analog inputs and outputs and depending on the configuration of the device a variety of modules for digital interfaces. With the corresponding analyzer software, fully automated acoustic measurements can be made. The measurement results can then be used for calculations and exported to a desired file format for further use [18].

### 2.2.2 APx1701 Transducer Test Interface

The APx1701 transducer test interface from Audio Precision is a combined power amplifier and microphone signal conditioning unit. It can be used as a power supply for pre-polarized measurement microphones (+24 V CCP) as well as for condenser microphones (+48 V phantom power). Via separate XLR and BNC jacks, the microphone signals can then be routed through to the APx525 audio analyzer. [19]

### 2.2.3 Ear Simulator

In order to be able to make meaningful measurements on in-ear headphones, it is necessary to properly simulate its acoustic surroundings, i.e., the human ear canal. For this purpose, a variety of ear simulators are available for use. For the work done in this thesis a GRAS RA0045 ear simulator was used. Its acoustic impedance is designed to closely match the



(a) Frequency response of the coupler, taken from [20]



(b) GRAS coupler

Figure 2.2: GRAS RA0045 Externally Polarized Ear Simulator

one of a human ear and therefore the coupler loads a headphone in a very similar way. Figure 2.2a shows its typical frequency response.

The ear simulator is mounted on a test jig that has a calibrated pressure microphone build in. The whole test setup is shown in figure 2.2b.

## 2.3 Microphones

For a good ANC performance, the right choice of the microphone is crucial. A good microphone has to have certain properties, which makes it suitable for a noise cancelling application. The large field of different types, however, is limited by size constraints and therefore only the small electric condenser microphones (ECMs) and the even smaller MEMS (Micro Electro-Mechanical System) microphones come into question.

The next two sections give a more detailed description of these two types and their most important properties.

### 2.3.1 Electret Condenser Microphones

Electret Condenser Microphones are a special version of the general condenser microphone where changes in sound pressure level are translated into changes of microphone capacitance. This is achieved through the deflection of one or both capacitor plates caused by a change in sound pressure level. Condenser microphones need a DC polarizing voltage for operation. To avoid the need for an external voltage, one capacitor plate can be coated with a prepolarized material, the so called electret. During manufacturing in a strong electric field and under high temperature, this material (usually PTFE) obtains a permanent electrostatic charge, which it keeps when it is cooled back down [21]. Figure 2.3 shows a

typical implementation of such a microphone where the electret coating is applied to the back plate of the head capacitor. The electret can also be used as the diaphragm of the microphone, but the higher mass, compared to materials typically used for diaphragms, potentially decreases HF performance.

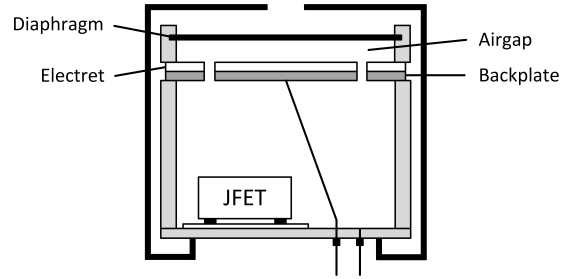


Figure 2.3: Cross section of an electret condenser microphone according to [2]

To obtain a usable output signal, usually the microphone capacitor is followed by a buffer circuit. This is done to avoid charging or discharging of the capacitor. A basic preamplifier circuit is shown in figure 2.4 utilizing a JFET for buffering.

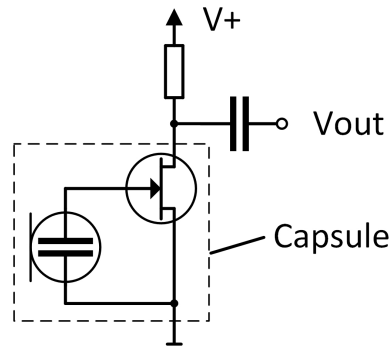


Figure 2.4: Commonly used preamplifier circuit for electret condenser microphones

The charge  $Q$  in the microphone capacitor remains constant due to the used electret material. Any excursion of the diaphragm  $d$  leads to a change in voltage  $U$  across the capacitor, as it is described by equation 2.7:

$$Q = C \cdot U = \frac{\epsilon \cdot A}{d} \cdot U \quad (2.7)$$

where  $C$  is the microphone capacitance,  $\epsilon$  is the absolute permittivity and  $A$  is the area of the capacitor plates.

An alternative method for generating the output signal is to use the changing capacitance to modulate an RF signal which can later be demodulated to deliver the desired signal.

### 2.3.2 MEMS Microphones

As their name suggests, these microphones are MEMS devices consisting of a variable MEMS capacitor and an ASIC (Application Specific Integrated Circuit) for signal conversion. Usually, the capacitor and the electronics are placed on two separate dies that are then wirebonded to a common substrate. This allows for a standard CMOS process being used for the ASIC, while the capacitor can be manufactured with an optimized MEMS process. The principle of operation is the same as in condenser microphones: incoming sound waves deflect the moveable plate of a capacitor resulting in a change of capacitance.

In figure 2.5, the cross section of a MEMS capacitor is shown. It consists of a fixed and a moveable plate made out of silicon. The fixed capacitor plate is perforated to allow the air to flow through. It is covered by an electrode to make it conductive. The second plate is moveable, because it is only fixed on one side allowing it to vibrate and to act as a membrane. The substrate under the membrane is etched away to allow the sound waves to enter.

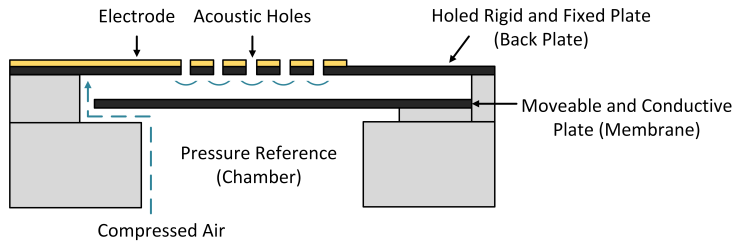


Figure 2.5: Cross section of a MEMS transducer according to [3]

The location of the sound inlet can either be on the bottom of the device, where its electric contacts are (bottom port device), or on the opposite side of it (top port device). The two configurations are depicted in figure 2.6. Bottom port devices usually have better acoustic properties due to the fact that the sensor is placed directly at the sound inlet of the package. This results in a small front volume causing the Helmholtz resonance to shift to higher frequencies granting a flatter frequency response. Also, the large back volume is beneficial, because it improves low frequency performance as well as the SNR of the device. However, the choice of which port type to use is mostly determined by the mounting in the final application.

To obtain a usable output signal from the varying MEMS capacitance, the change in capacitance needs to be converted into a change in voltage. To accomplish this, a dedicated ASIC is used, which is placed next to the MEMS device in the same package. The main parts of this ASIC are a charge pump for biasing and buffer circuitry to provide proper loading of the MEMS capacitor. Depending on whether an analog or digital microphone is used, the output signal will either be an analog one, or in the digital case, a PWM signal. Some types offer an I2S output instead of the PWM signal.

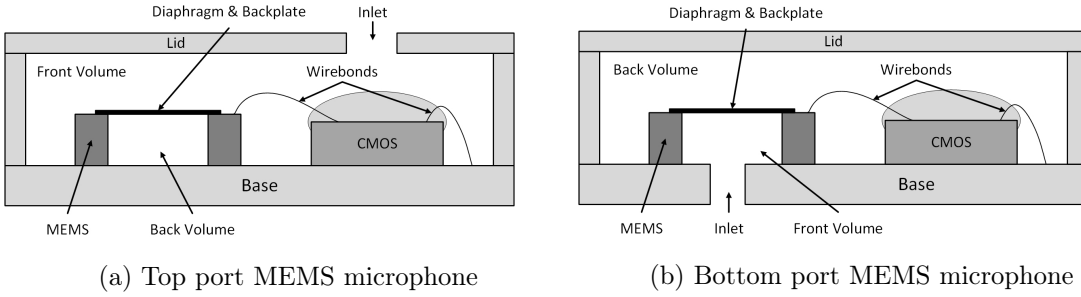


Figure 2.6: MEMS microphone types according to [4]

### 2.3.3 Important Properties for ANC

#### Frequency Response

Obviously the microphone’s magnitude response should be as flat as possible to allow accurate capturing of the noise. Another very important property of the microphone is its lower corner frequency which should be as low as possible for optimum performance. This is mainly due to the corresponding phase shift of already  $+45^\circ$  at the corner frequency (depicted in figure 2.7). Furthermore, small tolerances on the frequency response from microphone to microphone are desirable to ensure stable performance for the various devices.

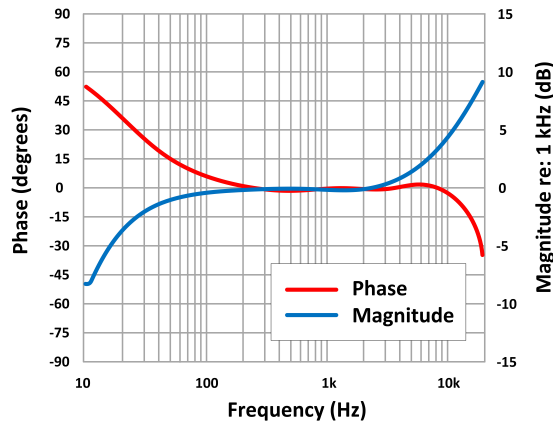


Figure 2.7: Example microphone phase and magnitude response according to [5]

#### Dynamic Range

The acoustic overload point (AOP) is an important metric for an ANC microphone. It specifies the sound pressure level at which the output signal of the microphone is distorted by a certain factor, usually 10%. Therefore, the AOP corresponds to the maximum output signal that the microphone can generate without excessive distortion. The magnitude of the smallest usable signal generated by the microphone can be considered to be equal to the

magnitude of the residual noise. The dynamic range of a microphone is the span between these minimum and maximum signals. It can be calculated from the relationship between sensitivity, SNR and AOP. This is depicted in figure 2.8.

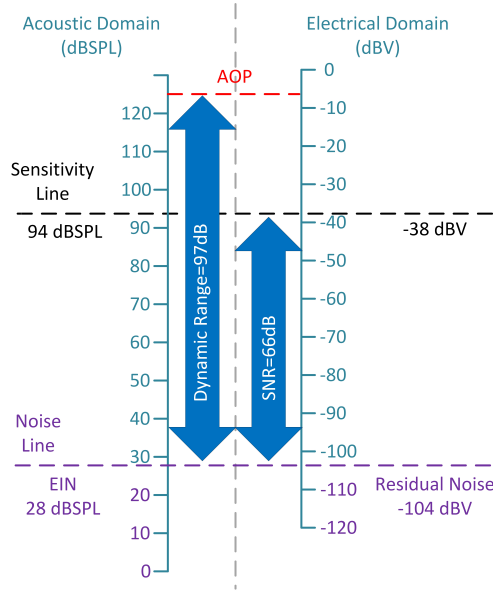


Figure 2.8: Determination of the dynamic range of a microphone according to [3]

### Group Delay

The group delay is defined as the negative derivative of the phase response as written in equation 2.8. It describes the time delay of the individual frequencies that is introduced as they are being picked up by the microphone. In general, this time delay is frequency-dependent which leads to a distortion of the waveform analog to the dispersion in optical systems. Due to the fact that in a microphone the output signal is always delayed to the input signal, the phase response  $\varphi(\omega)$  is a decreasing function and hence the group delay is always a positive number.

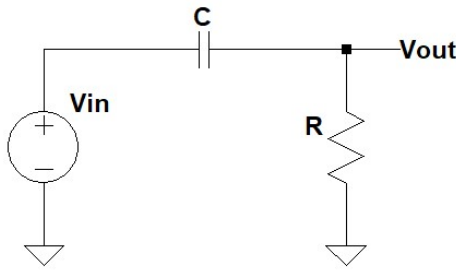
$$\tau_G = -\frac{d\varphi(\omega)}{d\omega} \tag{2.8}$$

### 2.3.4 Comparison

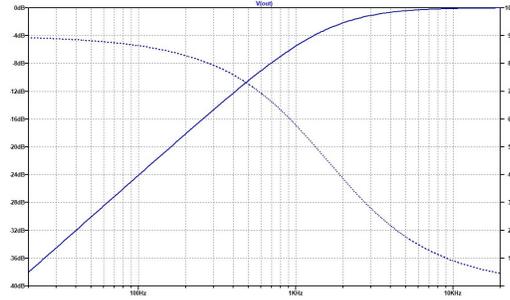
Table 2.1 gives a comparison of MEMS and electret microphone properties. Matched MEMS microphones with sensitivity matching are available granting much smaller tolerances of  $\pm 1$  dB. Thermal stability is much better over the operating temperature range, they can be reflow soldered and are not as susceptible to vibrations compared to their counterparts [22] [23]. ECMs, on the other hand, generally have a better low frequency behavior, widening the possible ANC bandwidth and potentially improving ANC performance.

Type	Therm. stability	Sensitivity	Low $f_{3dB}$	Reflow soldering	Vibration sensitivity
ECM	$\pm 4$ dB	$\pm 3$ dB	+	~	-
MEMS	$\pm 0.5$ dB	$\pm 1$ dB	~	+	+

Table 2.1: Comparison of MEMS and electret microphones for ANC applications



(a) Schematic



(b) Magnitude and phase response

Figure 2.9: Passive high pass filter

## 2.4 Analog Filters

The performance of analog active noise cancellation depends heavily on the ANC filter design. A good understanding of the basic filter topologies is therefore crucial. This section covers the basic filter blocks that will be used later in this work.

### 2.4.1 High Pass Filter

A voltage divider consisting of a capacitor and a resistor can be used to form a passive high pass filter. The schematic is shown in figure 2.9, where also the frequency response is plotted. Equation 2.9 is used to calculate the transfer function of such a filter from which the 3 dB corner frequency can be derived (equation 2.10). Initially, the phase shift is  $+90^\circ$  and with increasing frequency it approaches  $0^\circ$ . At the 3 dB corner frequency there is a  $+45^\circ$  phase shift.

$$\frac{V_{out}}{V_{in}} = \frac{j\omega RC}{1 + j\omega RC} \tag{2.9}$$

$$f_{3dB} = \frac{1}{2\pi RC} \tag{2.10}$$

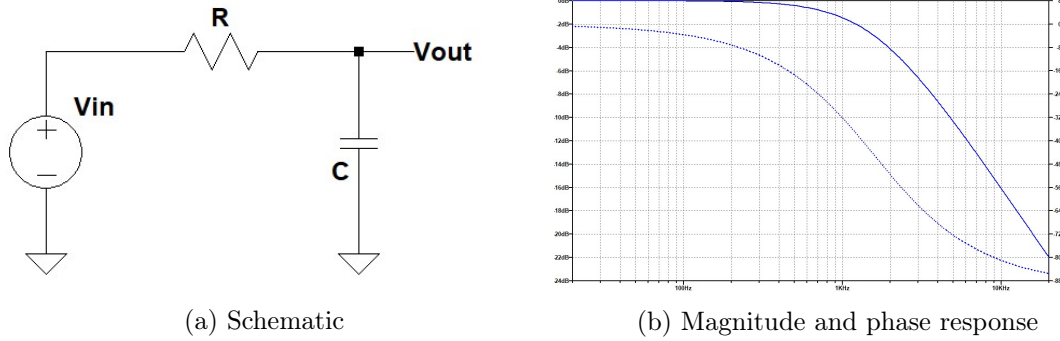


Figure 2.10: Passive low pass filter

## 2.4.2 Low Pass Filter

### Passive Low Pass Filter

If the order of components of a high pass filter is reversed, one obtains a passive low pass filter as depicted in figure 2.10. Equation 2.11 defines the transfer function of such a filter. The phase shift is initially  $0^\circ$  while it approaches  $-90^\circ$  with increasing frequency. Analog to the passive high pass filter, the 3 dB corner frequency can be calculated according to equation 2.12

$$\frac{V_{out}}{V_{in}} = \frac{1}{1 + j\omega RC} \quad (2.11)$$

$$f_{3dB} = \frac{1}{2\pi RC} \quad (2.12)$$

### Active Low Pass Filter

There are several ways how an active low pass filter can be formed. One is using a passive filter followed by a buffer circuit. Another one is using an inverting integrator circuit with a parallel feedback resistor to avoid saturation, also known as lossy integrator [24]. The transfer function is similar to the one for the passive filter but with an additional gain term (equation 2.13).

$$\frac{V_{out}}{V_{in}} = -\frac{R_2}{R_1} \cdot \frac{1}{1 + j\omega R_2 C_2} \quad (2.13)$$

$$f_{3dB} = \frac{1}{2\pi R_2 C_2} \quad (2.14)$$

Since it is based on an operational amplifier in inverting configuration, it shows a phase shift of  $180^\circ$  which approaches  $90^\circ$  for frequencies above the corner frequency. Schematic

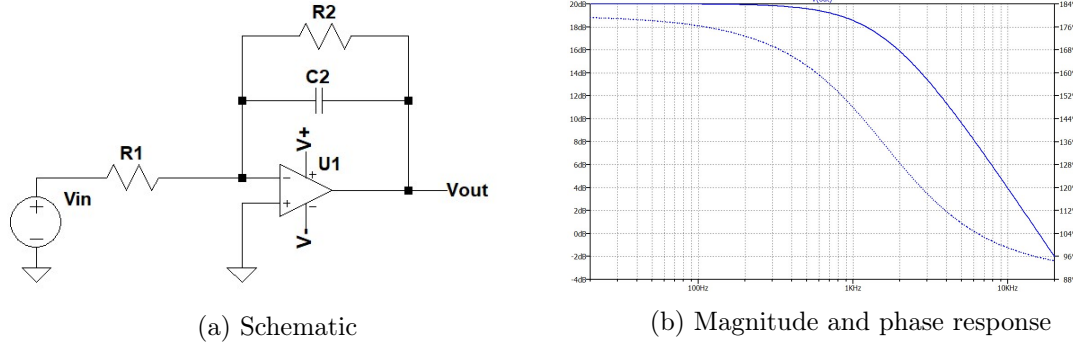


Figure 2.11: Lossy integrator as active low-pass filter

and frequency response of such a filter are shown in figure 2.11. The used component values were:  $R_1 = 1\text{ k}\Omega$ ,  $R_2 = 10\text{ k}\Omega$  and  $C_2 = 10\text{ nF}$ .

### 2.4.3 Shelving Filters

These types of filters allow to boost or attenuate signals over the whole range above or below the corner frequency by a fixed factor. Active shelving filters are based on operational amplifiers that can be either in inverting or non-inverting configuration. The gain in a non-inverting operational amplifier circuit is defined as  $A_{NINV} = 1 + \frac{R_f}{R_g}$  and can never be below  $1 \frac{V}{V}$  (0 dB). Circuits based on the inverting topology can also be used to attenuate signals. These types are briefly summarized below.

#### High Shelf Filter

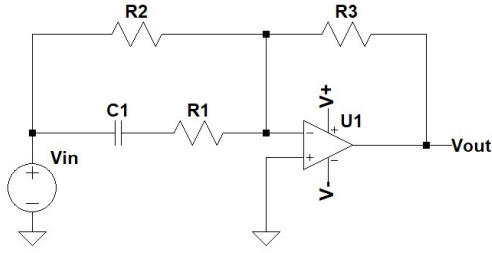
Figure 2.12a shows the schematic of an active high shelf filter. It can be viewed as an operational amplifier in inverting configuration with frequency dependent gain. The transfer function of the circuit is given by equation 2.15 which can be rewritten to equation 2.16.

$$\frac{V_{out}}{V_{in}} = -\frac{R_3}{R_2 \parallel (R_1 + \frac{1}{j\omega C_1})} \quad (2.15)$$

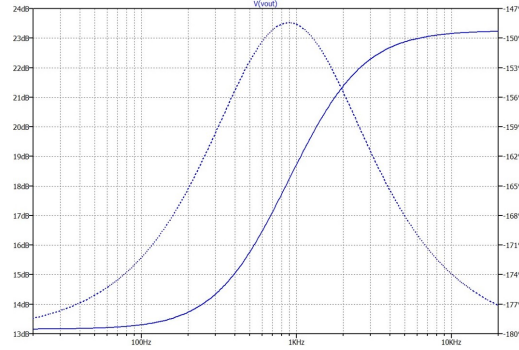
$$\frac{V_{out}}{V_{in}} = -\frac{R_3}{R_2} \cdot \frac{1 + j\omega(R_1 + R_2)C_1}{1 + j\omega R_1 C_1} \quad (2.16)$$

Below the corner frequency  $f_{C_{low}}$  (defined in equation 2.18) the path formed by  $C_1$  and  $R_1$  can be neglected. In this region the gain of the circuit is  $A_{low}$ .

$$A_{low} = \frac{R_3}{R_2} \quad (2.17)$$



(a) Schematic



(b) Magnitude and phase response

Figure 2.12: Active high shelf filter

$$f_{C_{low}} = \frac{1}{2\pi(R_1 + R_2)C_1} \quad (2.18)$$

Above  $f_{C_{high}}$  the gain of the circuit is  $A_{high}$ .

$$A_{high} = \frac{R_3}{R_1 \parallel R_2} \quad (2.19)$$

$$f_{C_{high}} = \frac{1}{2\pi R_1 C_1} \quad (2.20)$$

The magnitude and phase response of an active high shelf filter is shown in figure 2.12b for the values  $R_1 = 1 \text{ k}\Omega$ ,  $C_1 = 100 \text{ nF}$ ,  $R_2 = 2.2 \text{ k}\Omega$  and  $R_3 = 10 \text{ k}\Omega$ . Since the operational amplifier is in inverting configuration, the phase is at  $-180^\circ$  with a peak between the two corner frequencies  $f_{C_{low}}$  and  $f_{C_{high}}$ .

### Low Shelf Filter

The schematic of a low shelf filter is shown in figure 2.13a. It is based on an operational amplifier in inverting configuration. The transfer function of the filter can be calculated according to equation 2.21.

$$\frac{V_{out}}{V_{in}} = -\frac{R_2 \parallel (R_1 + \frac{1}{j\omega C_1})}{R_3} \quad (2.21)$$

$$\frac{V_{out}}{V_{in}} = -\frac{R_2}{R_3} \cdot \frac{1 + j\omega R_1 C_1}{1 + j\omega(R_1 + R_2)C_1} \quad (2.22)$$

Frequencies below  $f_{C_{low}}$  are amplified by a factor of  $A_{low}$ .

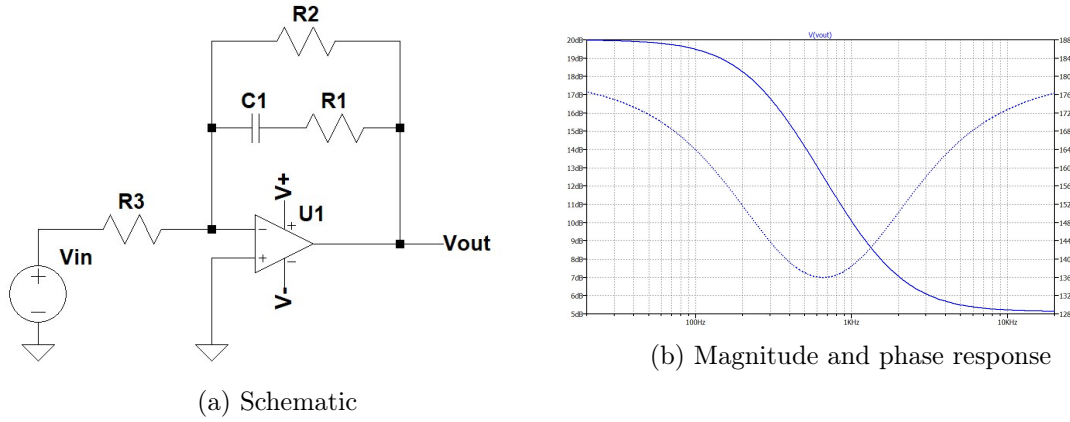


Figure 2.13: Active low shelf filter

$$A_{low} = \frac{R_2}{R_3} \quad (2.23)$$

$$f_{C_{low}} = \frac{1}{2\pi(R_1 + R_2)C_1} \quad (2.24)$$

For frequencies above  $f_{C_{high}}$  the gain changes to  $A_{high}$ .

$$A_{high} = \frac{R_1 \parallel R_2}{R_3} \quad (2.25)$$

$$f_{C_{high}} = \frac{1}{2\pi R_1 C_1} \quad (2.26)$$

The frequency response for a low shelf filter using the component values  $R_1 = 22 \text{ k}\Omega$ ,  $C_1 = 10 \text{ nF}$ ,  $R_2 = 100 \text{ k}\Omega$  and  $R_3 = 10 \text{ k}\Omega$  is depicted in figure 2.13b. As for the high shelf filter the phase is shifted by  $180^\circ$  over the whole region but with a notch between the two corner frequencies  $f_{C_{low}}$  and  $f_{C_{high}}$ .

#### 2.4.4 Notch Filter

A Twin-T notch filter with additional damping resistor  $R_d$  is shown in figure 2.14. Incrementing the value of  $R_d$  results in a stronger damping of the notch. Figure 2.15 shows the frequency response of the filter for the values of  $R = 10 \text{ k}\Omega$  and  $C = 10 \text{ nF}$ ,  $R_d$  is varied from  $1 \Omega$  to  $4 \text{ k}\Omega$ . At the notch frequency, which can be calculated according to equation 2.27, the phase shifts from  $-90^\circ$  to  $90^\circ$ .

$$f_{3dB} = \frac{1}{2\pi RC} \quad (2.27)$$

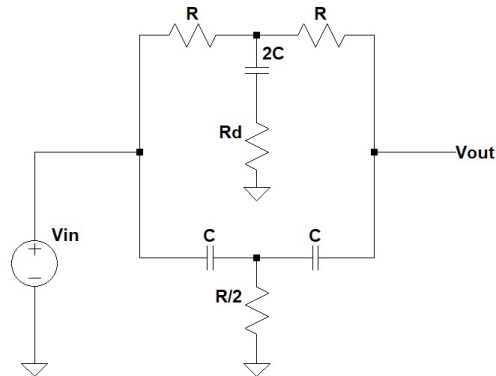


Figure 2.14: Schematic of a notch filter

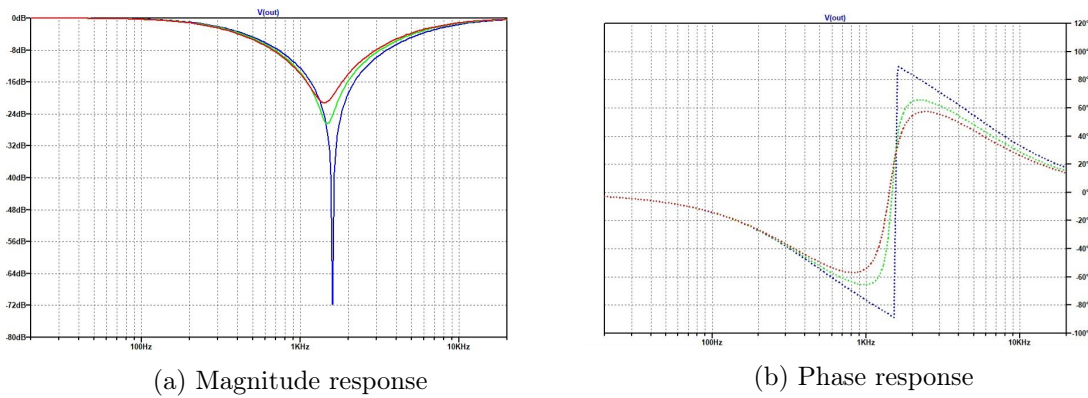


Figure 2.15: Frequency response of the notch filter for different values of  $R_d$

## 2.5 MEMS Speaker

For this work the USound MEMS speakers [6] will be used instead of electrodynamic or balanced armature speakers, which are commonly used in in-ear ANC applications. At the core of the speaker, cantilevers made out of piezoelectric material such as PZT (lead zirconate titanate) or AlN (aluminium nitride) are used. These materials have the property to shrink or expand in case an electric field is applied across them. A cantilever is formed by adding a layer of piezoelectric material on top of a silicon plate as shown in figure 2.16. The piezoelectric layer shrinks as soon as an electric field is applied, thus causing the cantilever to bend.

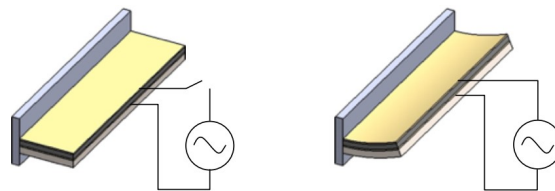


Figure 2.16: Bending of a piezoelectric cantilever due to an applied voltage, taken from [6]

To obtain a lateral movement multiple, cantilevers are connected to a central structure to form a so called MEMS motor as depicted in figure 2.17. The cantilevers are arranged in a symmetrical manner to ensure that the central structure or plate moves up and down.

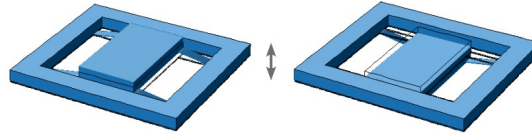


Figure 2.17: MEMS motor consisting of multiple cantilevers, taken from [6]

Finally, a membrane is attached to the plate to increase the moving area and thus to increase the amount of air that is being moved. The so formed MEMS speaker can be seen in figure 2.18. Since, in contrast to conventional speakers, no magnets and coils are being used, these speakers can be manufactured to be very thin and lightweight.



Figure 2.18: Membrane attached to MEMS motor to generate sound, taken from [6]

MEMS speakers are capacitive in nature, whereas a conventional electrodynamic speaker is an inductive device. The overall behavior of a MEMS speaker can be simulated with aid of the lumped parameter model as shown in figure 2.19. In the electrical domain the speaker is approximated as an ideal capacitor with an inductor in parallel.

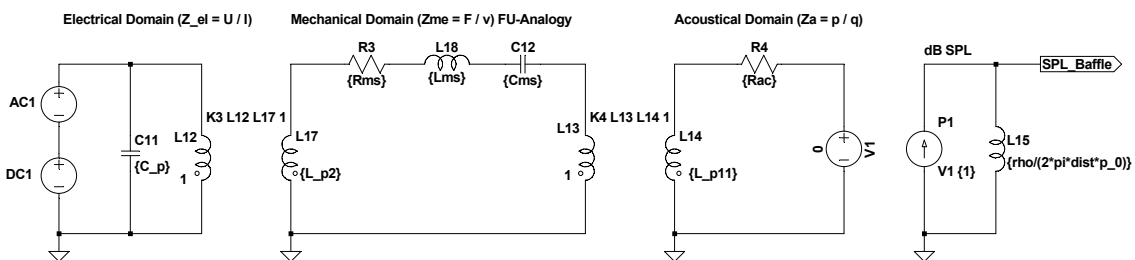


Figure 2.19: Electro-mechanical-acoustical spice model of a MEMS speaker

Due to the operation principle of MEMS speakers, they require special driving circuitry. For proper operation, the speaker must be DC biased so that  $V_{DC} \geq V_{PAC}$ .

## Chapter 3

# Active Noise Cancellation

### 3.1 ANC Topologies

The two main topologies used in ANC systems are feedforward and feedback systems. Their names indicate the signal flow from the ANC microphones in the system and determine the placement position of the ANC microphones.

#### 3.1.1 Feedforward

In the feedforward topology, the microphone is placed outside of the earcup of the headphone (see figure 3.1a). In this configuration, the microphone captures the surrounding noise some time before it arrives at the human ear. The ANC system then creates an anti-noise signal, which is played back over the speaker so that the noise reaching the ear and the produced anti-noise cancel out. Depending on the design, frequencies up to  $3\text{ kHz}$  can be canceled with this approach. A good sealing of the earphone to the ear is necessary to avoid additional noise from entering the earcup due to loose fit of the earphone. Since a feedforward system does not have a regulation loop to account for the additional noise, any change in wearing situation directly affects ANC performance. Another aspect that needs to be considered is the microphone exposure to the surroundings. Wind can cause problems when the microphone placement is not chosen carefully.

This topology can also be used to deliberately amplify the surrounding noise, which might be helpful in a situation where the listener wants to hear an announcement while wearing the earphones, for example.

#### 3.1.2 Feedback

Figure 3.1b shows a typical feedback topology where the microphone is placed between the loudspeaker and the human ear. Because of this, the microphone does not only record the noise, but also the music that is being played back by the loudspeaker. This signal is passed to the ANC circuitry, where it is filtered and fed back to the speaker. Due to this

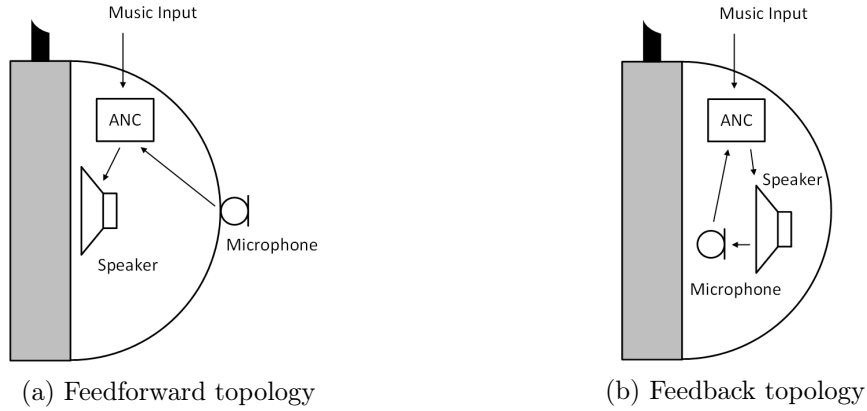


Figure 3.1: Feedforward and feedback ANC topologies

feedback loop, it is possible to account for small leakages introduced by a changing wearing situation. Another advantage comes with the fact that the microphone is placed inside the earcup causing wind noise not to be an issue. In comparison to feedforward systems, the low frequency performance is better, but the overall noise cancellation bandwidth is smaller (typically up to 1 kHz for analog systems)

### 3.1.3 Hybrid

Feedforward and feedback topology can also be combined into one system, which is referred to as a hybrid system. A hybrid system offers potentially the best performance of all systems. The downside is the higher complexity, cost and power consumption for such a system, since two microphones per channel are needed, making for a total of four microphones for an ANC headset. The block diagram of a hybrid system is shown in figure 3.2.

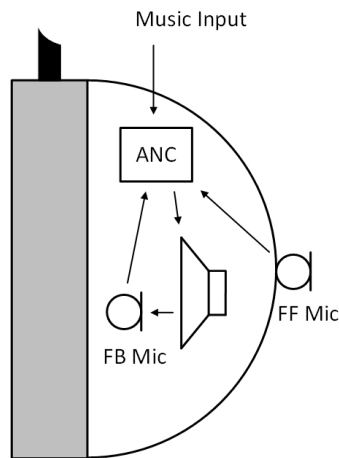


Figure 3.2: Hybrid ANC topology

## 3.2 Analog versus Digital ANC Systems

### 3.2.1 Analog Systems

The block diagram of an analog feedforward ANC system is shown in figure 3.3. Such a system consists of a microphone preamplifier, several stages of analog filters and a power amplifier driving the cancelling loudspeaker. Usually, these blocks, together with the microphone supply, are integrated into an ASIC to allow a small form factor of the system. The ANC filter response is defined by the choice of external circuitry, usually a large number of capacitors and resistors, which in combination with the integrated operational amplifiers form the individual filter stages. Therefore, the component tolerances directly influence the performance of an analog ANC system.

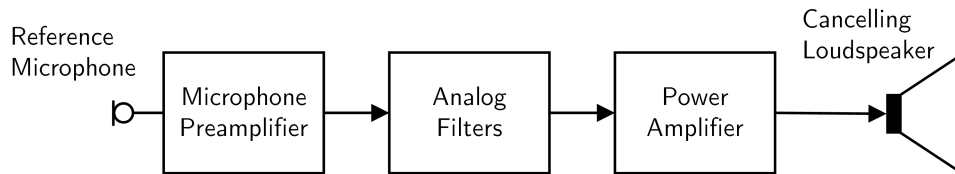


Figure 3.3: Block diagram of an analog feedforward ANC system

Since the whole signal path is purely analog, the latency of the cancelling signal is minimal.

### 3.2.2 Digital Systems

In contrast to an analog system, the electronic part of a digital ANC system consists of the following three main building blocks:

- A/D converters with anti-aliasing filters
- Microprocessors
- D/A converters with reconstruction filters

A typical digital feedforward ANC application for noise control in a duct is depicted in figure 3.4a from which the basic system model can be derived. It consists of a reference microphone, often also referred to as reference sensor that picks up the primary noise, an error microphone or error sensor to pick up the residual noise, a control unit that generates the cancellation signal and a loudspeaker also called secondary source which is used to create the anti-noise. As there is only one secondary source, this is a single channel system.

Figure 3.4b shows the corresponding system representation.  $P(z)$  models the path from reference sensor to error sensor,  $W(z)$  is a digital filter that is used to estimate the behavior of the unknown plant  $P(z)$ . Generally,  $P(z)$  is dynamic, therefore  $W(z)$  has to be an adaptive filter to be able to track the changes over time.

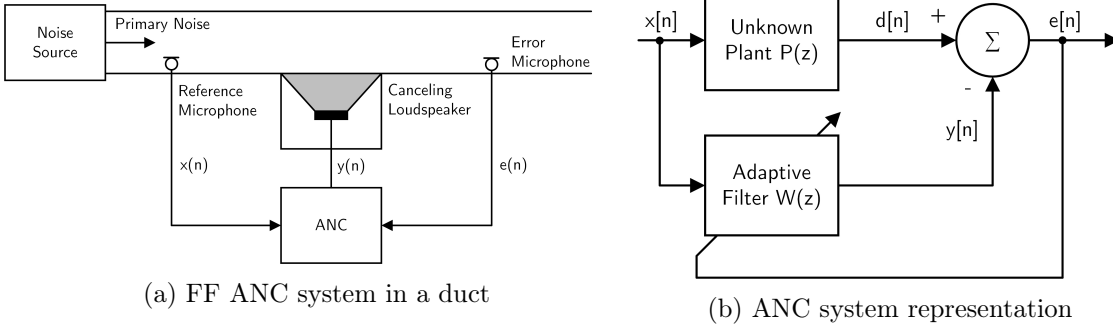


Figure 3.4: Digital feedforward system for noise control in a duct

**Filters**

The digital filter in the ANC system is used to create the control signal output from the reference signal input. For this, the reference input samples (both current and past) are multiplied with the coefficients of the filter and added up to generate the output signal.

**FIR Filters**

The most commonly used filter type for digital ANC is the finite impulse response (FIR) filter whose structure is shown in figure 3.5. The filter is described by equation 3.1, where  $y[n]$  is the filter output,  $w_i$  are the filter coefficients,  $N$  is the filter order and  $x[n - i]$  is the filter input delayed by  $i$  samples. These filters are best used in applications where tonal noise is to be reduced and where no acoustic feedback exists, meaning that the reference signal is not being affected by the control signal [12].

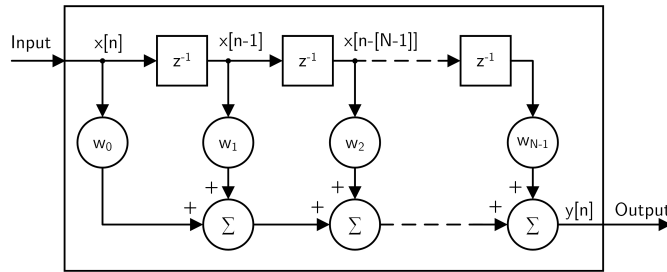


Figure 3.5: FIR filter structure

$$y[n] = \sum_{i=0}^{N-1} w_i \cdot x[n - i] \tag{3.1}$$

**IIR Filters**

In situations where acoustic feedback is a problem or when there are resonances in the system that shall be controlled, an infinite impulse response (IIR) filter is often used, since it offers the possibility to model the poles in such a system. Figure 3.6 depicts the structure of an IIR filter. It is described by equation 3.2, where  $y[n]$  is the filter output,  $a_i$  and  $b_i$  are the filter coefficients and  $x[n]$  is the filter input.

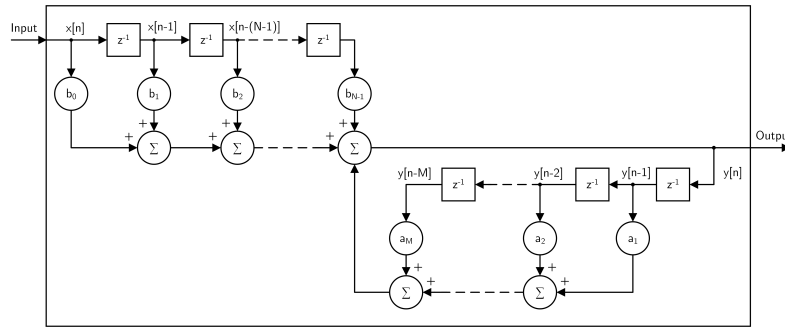


Figure 3.6: IIR filter structure

$$y[n] = \sum_{i=1}^M a_i \cdot y[n - i] + \sum_{j=0}^{N-1} b_j \cdot x[n - j] \tag{3.2}$$

Compared to FIR filters, IIR filters typically require fewer coefficients to model complex systems, therefore reducing the number of calculation steps and hence reducing the load on the microprocessor. The downside of IIR filters is their inherent instability and slower convergence [12].

**Algorithms**

A well-known algorithm for calculating the coefficients of an adaptive filter is the Least Mean Square algorithm (LMS), which has been used in telephone echo canceling systems for years [12]. A typical adaptive FIR filter is shown in figure 3.7.

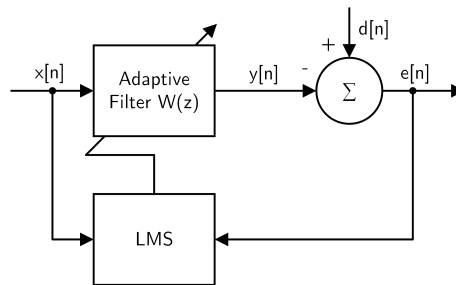


Figure 3.7: Typical adaptive filter

The adaptive FIR filter output  $y[n]$  is given by:

$$y[n] = \sum_{k=0}^{N-1} w_k[n]x[n-k] \quad (3.3)$$

where  $x[n]$  is the input signal and  $w_k[n]$  are FIR filter coefficients. The adaptive filter adjusts the filter coefficients  $w_k[n]$  in a way so that the square of the error signal  $e[n]$  is minimized. The error signal is given by:

$$e[n] = d[n] - y[n] = d[n] - \sum_{k=0}^{N-1} w_k[n]x[n-k] \quad (3.4)$$

And hence the squared error signal is:

$$(e[n])^2 = \left( d[n] - \sum_{k=0}^{N-1} w_k[n]x[n-k] \right)^2 \quad (3.5)$$

The steepest descent optimization method can be used to minimize the squared error signal  $(e[n])^2$ . This is done by adding a portion of the negative gradient of  $(e[n])^2$  to the previous coefficients  $w_k[n]$  [25].

$$w_k[n+1] = w_k[n] - \frac{\mu}{2} \frac{\partial (e[n])^2}{\partial w_k[n]}, \quad k = 0, 1, \dots, N-1 \quad (3.6)$$

where  $w_k[n+1]$  are the next filter coefficients,  $w_k[n]$  are the current coefficients and  $\mu$  is an empirically chosen value for the step size.

The derivative of the squared error signal with respect to the  $m$ -th coefficient is:

$$\begin{aligned} \frac{\partial (e[n])^2}{\partial w_m[n]} &= \frac{\partial}{\partial w_m[n]} \left( d[n] - \sum_{k=0}^{N-1} w_k[n]x[n-k] \right)^2 = \\ &= -2 \left( d[n] - \sum_{k=0}^{N-1} w_k[n]x[n-k] \right) x[n-m] = -2e[n]x[n-m] \end{aligned} \quad (3.7)$$

Considering the derivative with respect to the  $k$ -th coefficient equation 3.7 can be rewritten to:

$$\frac{\partial (e[n])^2}{\partial w_k[n]} = -2e[n]x[n-k] \quad (3.8)$$

By inserting equation 3.8 to equation 3.6 the LMS algorithm can be expressed as:

$$w_k[n+1] = w_k[n] + \mu e[n] x[n-k], \quad k = 0, 1, \dots, N-1 \quad (3.9)$$

The LMS algorithm can also be written in matrix form:

$$\mathbf{w}[n+1] = \mathbf{w}[n] + \mu \mathbf{x}[n] e[n] \quad (3.10)$$

with  $\mathbf{w}[n] = [w_0[n] \ w_1[n] \ \dots \ w_{N-1}[n]]^T$  and  $\mathbf{x}[n] = [x[n] \ x[n-1] \ \dots \ x[n-(N-1)]]^T$

In an active noise cancellation system additionally the secondary path transfer function  $S(z)$  needs to be considered.  $S(z)$  includes the D/A conversion of the control signal, loudspeaker with amplifier, acoustic path from loudspeaker to error sensor and finally the A/D conversion of the error signal. A system model considering  $S(z)$  is shown in figure 3.8a.

The z-transform of the error signal in figure 3.8a can be calculated:

$$E(z) = [P(z) - S(z)W(z)] X(z) \quad (3.11)$$

Under the assumption that  $E(z) = 0$  for  $X(z) \neq 0$ , the optimal transfer function  $W^o(z)$  is obtained:

$$W^o(z) = \frac{P(z)}{S(z)} \quad (3.12)$$

This implies that the adaptive filter  $W(z)$  needs to model both  $P(z)$  and  $1/S(z)$ .

The addition of  $S(z)$  into a controller using the LMS algorithm generally causes instability because the error signal and the reference signal are not correctly aligned in time any more [26]. Therefore, active noise cancellation applications very often use a derivation of the standard LMS algorithm, the so-called filtered-X LMS algorithm (FXLMS), which takes account of the secondary path transfer function  $S(z)$ . This is achieved by filtering the reference signal with an estimate of the secondary path filter  $\hat{S}(z)$  before sending it to the weight update block. Such a system using the FXLMS is shown in figure 3.8b.

The FXLMS algorithm can be expressed as [26]:

$$\mathbf{w}[n+1] = \mathbf{w}[n] + \mu \mathbf{x}'[n] e[n] \quad (3.13)$$

where  $n$  is the time index,  $\mathbf{w}[n]$  is the coefficient vector of  $W[z]$ ,  $\mu$  is the step size,  $e[n]$  is the remaining error signal and  $\mathbf{x}'[n]$  is

$$\mathbf{x}'[n] = \hat{s}[n] * \mathbf{x}[n] \quad (3.14)$$

with  $\hat{s}[n]$  being the impulse response of the estimated secondary path filter  $S(z)$  and  $x[n]$  being the reference signal.

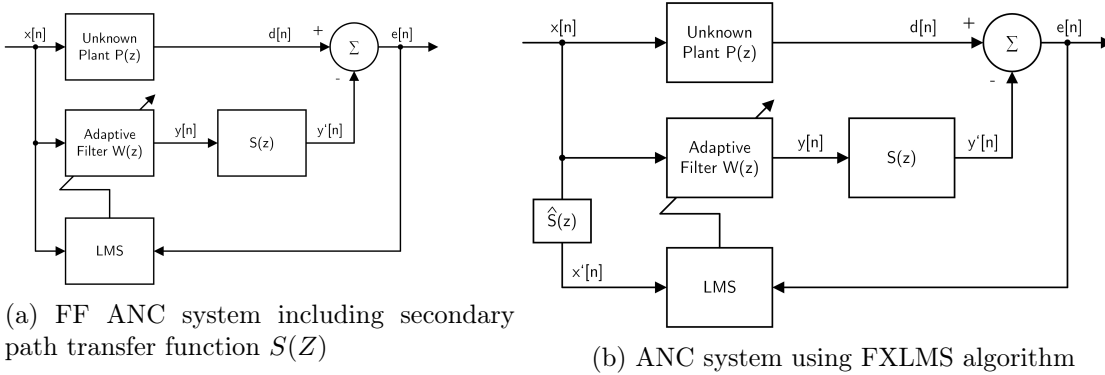


Figure 3.8: Digital feedforward system using the FXLMS algorithm for noise control in a duct

Parameter	Analog ANC	Digital ANC
Latency	+	-
Power consumption	+	-
Accuracy	-	+
Flexibility	-	+
Time to market	-	+

Table 3.1: Comparison of analog and digital ANC systems

### 3.2.3 Comparison

Table 3.1 shows a comparison of analog and digital ANC systems. Digital systems have an inherent latency that is caused by A/D and D/A conversion as well as by time needed for signal processing which limits the bandwidth of the system [27]. In an analog system, on the other hand, there is practically no delay from signal input to output. As in an analog system the filter characteristics are determined by passive components, these characteristics are not fixed, but vary from part to part because of the component tolerances. Analog systems also generally have a lower power consumption compared to their digital counterparts. For a digital system, the power consumption strongly depends on the individual application and scales with sampling rate. A huge advantage of digital systems is their flexibility and the possibility to implement complex filter structures. Filter coefficients can be changed instantly, which allows the implementation of adaptive filters and is beneficial for a fast design optimization process.

## 3.3 ANC Headphones on the Market

In this section, an overview of the currently commercially available ANC headphones is given. The devices are sorted depending on the headphone type (over-the-ear and in-ear) and further divided into subgroups depending on the connectivity (wired and wireless). The manufacturer suggested retail price (MSRP) is stated whenever available, the retail

Model	Manufacturer	Battery life	Price	Comments
MDR-ZX110NA	Sony	80 h	60 €	
Blackwire 7225	Plantronics	-	150 €	On-ear USB headset

Table 3.2: Available wired over-the-ear ANC headphones

price is used in cases when it was not possible to find the MSRP. All prices have been rounded up to the nearest integer value. Furthermore, the battery life for music playback with ANC turned on is stated whenever the information was available.

Unfortunately, the manufacturers do not provide any comparable ANC performance data and often only state the peak performance without mentioning the affected frequency range. Therefore, a performance comparison would only be possible by benchmarking the individual products under the same conditions.

### 3.3.1 Over-the-Ear Headphones

#### Wired

As the trend goes towards wireless applications, the availability of wired headphones is becoming a scarcity these days. Table 3.2 lists the only two available devices.

#### Wireless

There are plenty of wireless ANC over-the-ear headphones available on the market, as almost every manufacturer offers devices with noise cancellation functionality. Table 3.3 lists some of the popular models sorted in alphabetical order with respect to the manufacturer. All of the devices support Bluetooth and offer the possibility for taking phone calls. The price span ranges from 129 € to 800 €, with 331 € being the average cost of such a device. Also, in terms of battery life, there are big differences with an average battery life of approximately 26 h.

### 3.3.2 In-Ear Headphones

#### Wired

As with the over-ear headphones, the wired in-ear counterparts are a minority. Table 3.4 lists the available devices. Both the *Beoplay E4* and the *Quiet Comfort 20* have been on the market for some years now without being replaced by an updated wired version. The manufacturers have instead released several wireless ANC headphones.

Model	Manufacturer	Battery life	Price
N60NC Wireless	AKG	15 h	299 €
N700NC	AKG	23 h	349 €
ATH-ANC700BT	Audio Technica	25 h	169 €
ATH-ANC900BT	Audio Technica	35 h	269 €
H8i	Bang & Olufsen	30 h	400 €
H9 3rd Gen	Bang & Olufsen	25 h	500 €
Beoplay H95	Bang & Olufsen	38 h	800 €
QuietComfort 35 II	Bose	20 h	289 €
Noise Cancelling Headphones 700	Bose	20 h	399 €
Evolve2 85	Jabra	32 h	543 €
Evolve 75	Jabra	13 h	340 €
TUNE 750BTNC	JBL	15 h	129 €
Club 950NC	JBL	22 h	249 €
BT 220 NC	Phiaton	14 h	159 €
900 Legacy	Phiaton	43 h	249 €
HD 458BT	Sennheiser	30 h	199 €
Momentum 3 Wireless	Sennheiser	17 h	399 €
WH-910N	Sony	35 h	299 €
WH-710N	Sony	35 h	149 €
WH-1000XM3	Sony	30 h	379 €
WH-1000XM4	Sony	30 h	379 €

Table 3.3: Available wireless over-the-ear ANC headphones

Model	Manufacturer	Playtime	Price	Comments
Beoplay E4	Bang & Olufsen	20 h	250 €	introduced in 2017
QuietComfort 20	Bose	16 h	180 €	introduced in 2015
TT-EP002	TaoTronics	15 h	39 €	

Table 3.4: Available wired in-ear ANC headphones

## Wireless

The recent trend in wireless in-ear devices is towards true wireless stereo (TWS) headphones with ANC functionality. This is strongly driven by the availability of ultra-compact SoCs such as the Qualcomm QCC51xx series that offer integrated digital noise cancellation allowing for feedforward, feedback and hybrid topologies [28]. Nevertheless, there are still wireless devices on the market that have a wired connection between the two earphones, so called neckband headphones. Table 3.5 gives an overview of the available wireless in-ear headphones.

For TWS earphones, the battery life is stated as battery life of one charge of the earphones plus potential extra play time due to recharging in the provided charging case. The battery life for one charge ranges from 4 h up to 9 h and is 6 h in average over the TWS devices, while the price ranges from 89 € to 299 € with an average of 200 €.

Model	Manufacturer	Battery life	Price	Comments
ATH-ANC100BT	Audio Technica	10 h	99 €	
Evolve 75e	Jabra	14 h	252 €	Neckband type
2 BT 220 NC	Phiaton	9 h	120 €	Supports NFC
WI-C600N	Sony	6.5 h	149 €	Neckband type
WI-1000XM2	Sony	10 h	329 €	Neckband type
AirPods Pro	Apple	4.5 h + 19.5 h	240 €	TWS
ATH-ANC300TW	Audio Technica	4.5 h + 13.5 h	229 €	TWS
QuietComfort Earbuds	Bose	6 h + 12 h	280 €	TWS
FreeBuds 3	Huawei	4 h + 16 h	89 €	TWS
Elite 75t	Jabra	5.5 h + 18.5 h	130 €	TWS
LIVE FREE NC+ TWS	JBL	6 h + 12 h	159 €	TWS
Reflect Mini NC	JBL	6 h + 12 h	149 €	TWS
Galaxy Buds Life	Samsung	4 h + 15 h	109 €	TWS
WF-1000XM3	Sony	6 h + 18 h	249 €	TWS
WF-SP800N	Sony	9 h + 9 h	199 €	TWS
Momentum True Wireless 2	Sennheiser	7 h + 21 h	299 €	TWS
EAH-AZ70W	Technics	6.5 h + 13 h	279 €	TWS

Table 3.5: Available wireless in-ear ANC headphones

The wireless neckband type earphones, on the other hand, offer a higher battery life of 10 h on average and are in the same price range.

### 3.3.3 Summary

The headphone industry is expanding rapidly with true wireless earbuds being the fastest growing branch of devices [29]. The ability of a device to cancel ambient noise is an increasingly important purchase criterion and the market share of ANC headphones is expected to rise in the coming years.

Most of the commercially available noise canceling headphones are wireless devices with Bluetooth capability that also allow phone calls to be taken on the device. As wearing comfort is a major point to consider, wired ANC headphones are expected to become even rarer. ANC is predicted to be a key differentiator in in-ear TWS devices in the future.

## Chapter 4

# Development of ANC Demonstrator

### 4.1 Earphones

Starting point for the design of the ANC demonstrator is an already existing earphone design. The in-ear headphones used with the USound Megaclite reference design are going to be used and modified to include microphones for ANC. Megaclite is a USB-C headset featuring the USound piezoelectric MEMS speakers. Version 2 is shown in figure 4.1. The electronic part includes a DSP for audio filtering, buttons for volume control as well as play/pause and two LM48580 speaker amplifiers from Texas Instruments.

### 4.2 MEMS Speaker Driver

Since the USound Ganymede speakers are capacitive MEMS speakers, a dedicated driver circuitry is needed for proper operation. For this work the Texas Instruments LM48560 ceramic speaker driver IC is used. It is a class H amplifier with integrated boost converter in a 1.97 mm x 1.97 mm BGA package. Figure 4.2 shows the schematic of the LM48560



Figure 4.1: Megaclite USB-C headset

with the necessary external components.

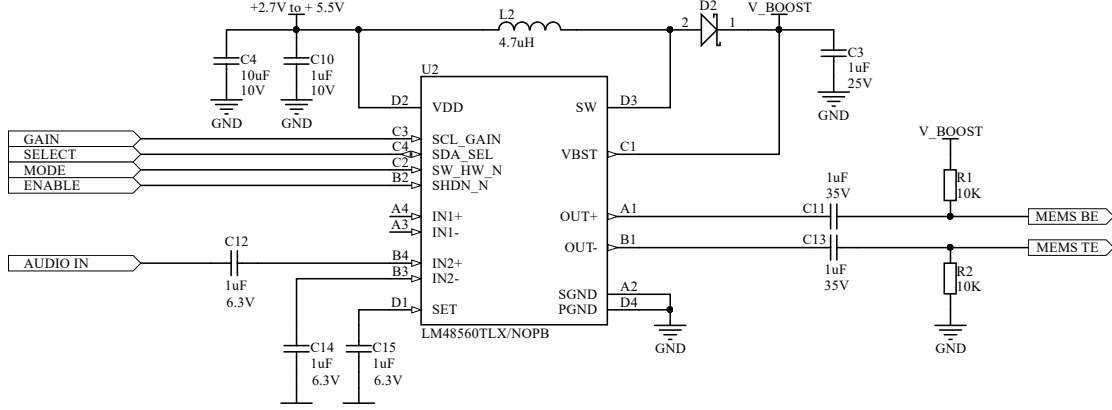


Figure 4.2: LM48560 speaker driver IC with necessary passive components

The LM48560 can either operate in software mode or in hardware mode depending on the state of the SW/HW pin. It offers two differential input pairs of which one needs to be selected by applying the appropriate voltage to the SEL pin.

For this work, the amplifier is controlled via the hardware mode and the second input pair is used in single-ended configuration. Therefore, the inverting input IN2- is tied to GND via an  $1\ \mu\text{F}$  capacitor. The positive speaker terminal is tied to  $V_{Boost}$  via a  $10\ \text{k}\Omega$  resistor and a  $1\ \mu\text{F}$  capacitor is used to block the DC voltage from the amplifier outputs.  $V_{Boost}$  is the internal boost voltage of the amplifier and it is nominally  $6\ \text{V}$ . As soon as the amplifier output increases above  $3\ V_{PP}$ , the boost voltage tracks the amplifier output.  $V_{Boost}$  reaches its maximum of  $15\ \text{V}$  at an output voltage of  $30\ V_{PP}$ . This provides the necessary DC bias for the operation of the MEMS speaker. Alternatively, a constant DC voltage of  $15\ \text{V}$  generated by a separate boost converter, can be applied instead.

The output circuitry forms two high pass filters with corner frequencies of  $15.9\ \text{Hz}$  each for the individual amplifier outputs. The gain of the amplifier is determined by the configuration of the gain pin. When input 2 is used, the gain can be set to be  $24\ \text{dB}$  or  $30\ \text{dB}$  by connecting it to GND or pulling it to VDD.

### 4.3 USound Ananke Board

As the basis for the ANC demonstrator, the Ananke board from USound was chosen. It was designed as an evaluation platform for MEMS speakers and features a programmable DSP that allows for the implementation of customized audio filters. An ADAU1401 from Analog Devices is used for this purpose. Stereo audio connection can either be established via  $3.5\ \text{mm}$  jack or via an integrated Bluetooth module. A pair of LM48560 class H drivers are used as audio amplifiers, making an output voltage swing from  $0\ \text{V}$  to about  $30\ \text{V}$  possible. The block diagram is depicted in figure 4.3.

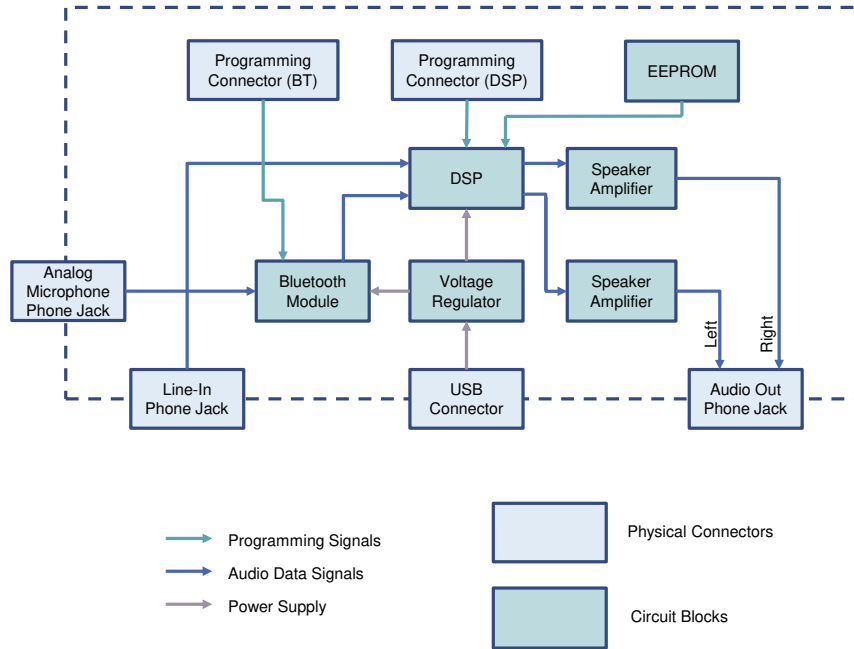


Figure 4.3: Block diagram of the Ananke evaluation board

	Manufacturer	Topology	Output	Package [mm]
AS3412	ams	FF	2 x SE / 1 x BTL	WL-CSP25 (2.2 x 2.2)
AS3415	ams	FF	2 x SE / 1 x BTL	QFN-32 (5 x 5)
AS3421	ams	FF	2 x SE / 1 x BTL	QFN-24 (4 x 4)
AS3422	ams	FB (FF)	2 x SE / 1 x BTL	QFN-32 (5 x 5)
AS3435	ams	FB (FF)	2 x SE / 1 x BTL	QFN-36 (5 x 5)
MAX9895A	Maxim	FF	2 x SE	36-WLP (2.7 x 2.7)
NE58633	NXP	FB (FF)	1 x BTL	HVQFN32 (5 x 5)

Table 4.1: Comparison of available noise cancelling ICs

## 4.4 Noise Cancelling IC AS3435

For the implementation of the ANC functionality in the demonstrator, a readily available analog solution was sought. Currently, a handful of manufacturers offer such a solution based upon dedicated so called "noise cancelling" IC's. They usually incorporate a charge pump for microphone supply, low noise operational amplifiers and a speaker driver output stage. Table 4.1 lists the investigated devices and gives a comparison in terms of supported ANC topology, output structure and size. Devices that support the feedback topology offer two operational amplifiers per channel for implementation of the ANC filter and can also be used in a feedforward architecture. Devices that only support the feedforward topology provide one amplifier per channel and therefore the more complex filtering necessary for hybrid ANC can't be implemented.

After a comparison, the decision was made to go for the AS3435 from ams since it allows the implementation of all ANC topologies and a good evaluation environment is available. The NE58633 from NXP Semiconductors was already discontinued. In figure 4.4, the block diagram of the chosen AS3435 IC is shown.

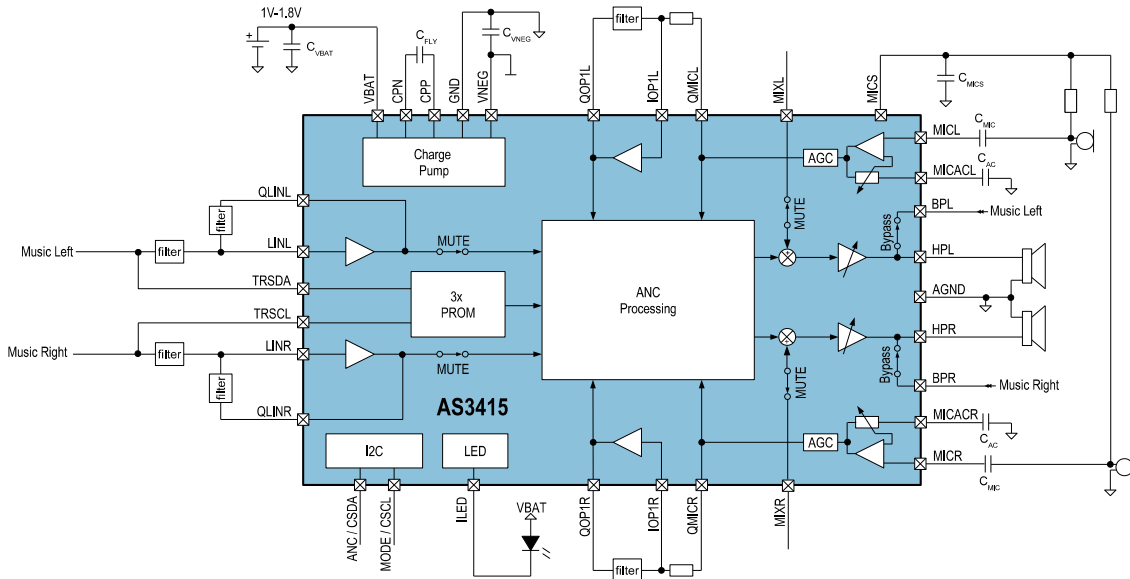


Figure 4.4: AS3435 Block diagram taken from the datasheet [7]

The AS3435 consists of a microphone interface which offers a supply voltage of typically 2.7 V supporting both ECM and MEMS microphones. The chip runs on a single supply voltage that can be in the range of 1 V to 1.8 V. It features two low noise microphone preamplifiers and is programmable via an I2C interface. The preamplifier gain can also be stored in an OTP ROM, which is useful for production trimming. Two operational amplifiers per channel are provided for ANC filtering, the filters itself have to be implemented using external resistors and capacitors. The IC can be used to realize a feedforward or feedback ANC stereo headphone or it can be used for the implementation of a hybrid architecture. This, however, would make the use of two AS3435 necessary, one for each channel. The output structure is designed for the use with electrodynamic speakers, both single ended operation or bridge tied load configuration is possible.

The noise canceling IC offers a line input for audio signals. The input stage is an inverting amplifier and its output and the inverting input are accessible via pins, while the non-inverting input is tied to GND internally. This allows for external configuration of input gain as well as the implementation of simple EQ circuits for the line input. The music input signal is then routed through the headphone amplifier to the HP outputs of the IC. The integrated headphone amplifier is designed to drive electrodynamic speakers and is not suitable for MEMS speakers. Therefore, a separate speaker amplifier needs to be used.

## 4.5 The Proposed Concept

For this work, an ANC implementation based on the AS3435 noise cancelling IC is proposed. The setup will be built around the readily available AS3435 evaluation board, which comes with a dedicated software for configuring the device and makes the necessary interconnections as easy as possible. To determine the best performing ANC topology, two prototype systems are investigated, one in feedback and one in feedforward architecture. A modified Megaclite earphone is manufactured and fitted with a variety of different microphones. ECM and MEMS microphones are then compared to find the most suitable one for the application. Due to the fact that the AS3435 is designed for the use with conventional speakers, its headphone amplifier cannot be used to drive the Megaclite earphones. Therefore, a USound Ananke board is used to drive the MEMS speakers.

### 4.5.1 Audio Signal Path

For the routing of the audio signal in the demonstrator, there are two options that need to be evaluated:

- Option 1: the audio signal is routed through the AS3435 to the LM48560's non-inverting input
- Option 2: the audio signal is routed directly to the LM48560's inverting input

#### Option 1: AS3435 in Audio Signal Path

The audio signal is routed through the AS3435, where it is added to the filtered ANC microphone signal. It passes the headphone amplifier and is then sent to the LM48560's non-inverting input as shown in figure 4.5. The LM48560 is used in single-ended configuration, the inverting input is connected via a capacitor to GND.

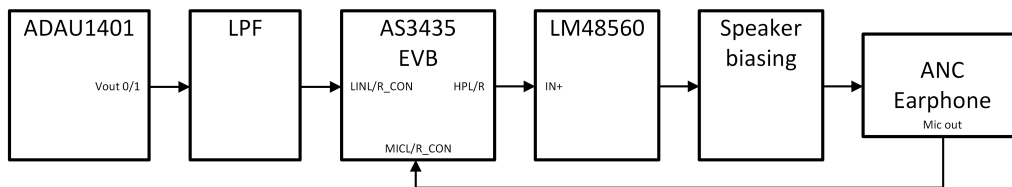


Figure 4.5: Option 1: routing audio through the AS3435

The datasheet of the AS3435 only specifies a minimum load impedance of  $16\ \Omega$  and does not specify a maximum load impedance [7]. Therefore, it can be expected that it can drive the LM48560 speaker driver with a typical input impedance of  $50\ \text{k}\Omega$  [30].

In order to pass the music signal through the AS3435 evaluation board, the line input gain needs to be set by soldering resistors on the board. The line input stage operates as an inverting amplifier and by setting both the input resistor and the feedback resistor to  $10\ \text{k}\Omega$  the gain of the stage becomes  $-1\ \frac{V}{V}$ .

### Option 2: AS3435 not in Audio Signal Path

The audio signal can be routed directly to the LM48560's inverting input omitting the AS3435. The filtered ANC microphone signal is routed from the headphone output of the AS3435 to the LM48560's non-inverting input. The music signal is then subtracted from the filtered ANC microphone signal in the LM48560, which is used in differential mode. This can also be interpreted as adding the inverted music signal to the filtered ANC microphone signal. A block diagram of the routing is shown in figure 4.6.

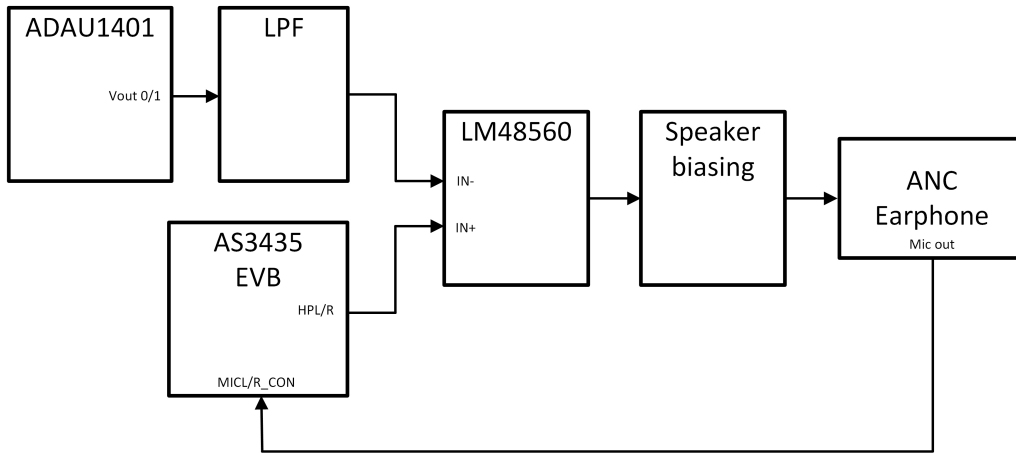


Figure 4.6: Option 2: routing audio directly to the LM48560

### Comparison

To evaluate the impact on the audio quality of the two routing options, the electrical THD+N and the RMS level at the speaker outputs of the LM48560 were measured. The APx audio analyzer was used as the signal source, the bandwidth was set to 45 kHz. A 22 nF capacitor was used as a load for the speaker amplifiers to make the measurements as comparable as possible. The audio performance was measured for a relatively low speaker voltage of 1.1 V<sub>rms</sub> and a high speaker voltage of 9 V<sub>rms</sub>. As the measurement results in figure 4.7 show, the THD+N is very similar for the routing options and also similar to the THD+N of the LM48560 alone in single-ended configuration. The only difference was that in case of option 1, a slightly higher input voltage had to be used to achieve the desired output level. Since the gain of the audio input signal can be easily adjusted in the ADAU1401, the routing option 1 was chosen for the demonstrator.

## 4.6 Feedback System

### 4.6.1 The Prototype

Using the feedback topology in a small earphone is challenging because space is very limited. This becomes apparent when looking at the 3d model of the Megaclite earphone

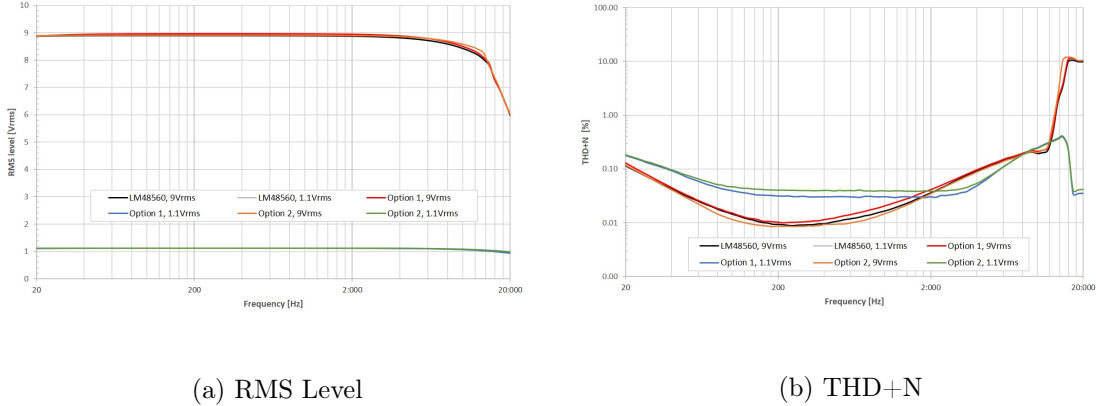


Figure 4.7: Impact of AS3435 noise cancelling IC on audio performance. Measured LM48560 output voltage with 22 nF capacitor as load for speaker voltages of 1.1 Vrms and 9 Vrms

depicted in figure 4.8a. Placing the microphone inside of the housing was not feasible and consequently a different approach had to be taken. The idea was to implement an additional venting hole that connects the volume between speaker and ear with the inlet of the feedback microphone which now can be placed on the outside of the housing.

Figure 4.8b shows a crosscut of this modified earphone. The orange cuboid is used to symbolize the feedback microphone that is glued to the shell. It is of importance that the gluing is absolutely airtight to ensure the pressure chamber effect continues to take place. The spiral tube that can be seen (the one that the vent runs off from) is the channel connecting speaker to earphone outlet. Its shape is spiraled to elongate the channel. This is deliberately done to push resonances in the earphone to a lower frequency, which in turn increases SPL at these frequencies.

Due to its small outer dimensions, the SPH1642 from Knowles was chosen as feedback microphone. It is a top port MEMS microphone with a lower cutoff frequency at 55 Hz, a SNR of 65 dB at 1 kHz and an AOP at 124 dB SPL [31].

### 4.6.2 Earphone Characterization

Prior to the actual system implementation, the earphone needs to be characterized. For feedback systems, this is done by making an open loop measurement between the speaker and the microphone in the earphone. The measurement setup for the characterization is shown in figure 4.9.

A sine sweep over the relevant audio range of 20 Hz to 20 kHz is produced by the APx525 and played back via the speaker in the earphone. This signal is then picked up by the feedback microphone and the reference microphone in the acoustic coupler. The two microphone signals are then routed to the inputs of the APx525, where the respective gain and phase responses are measured. Out of this measurement data, the necessary feedback

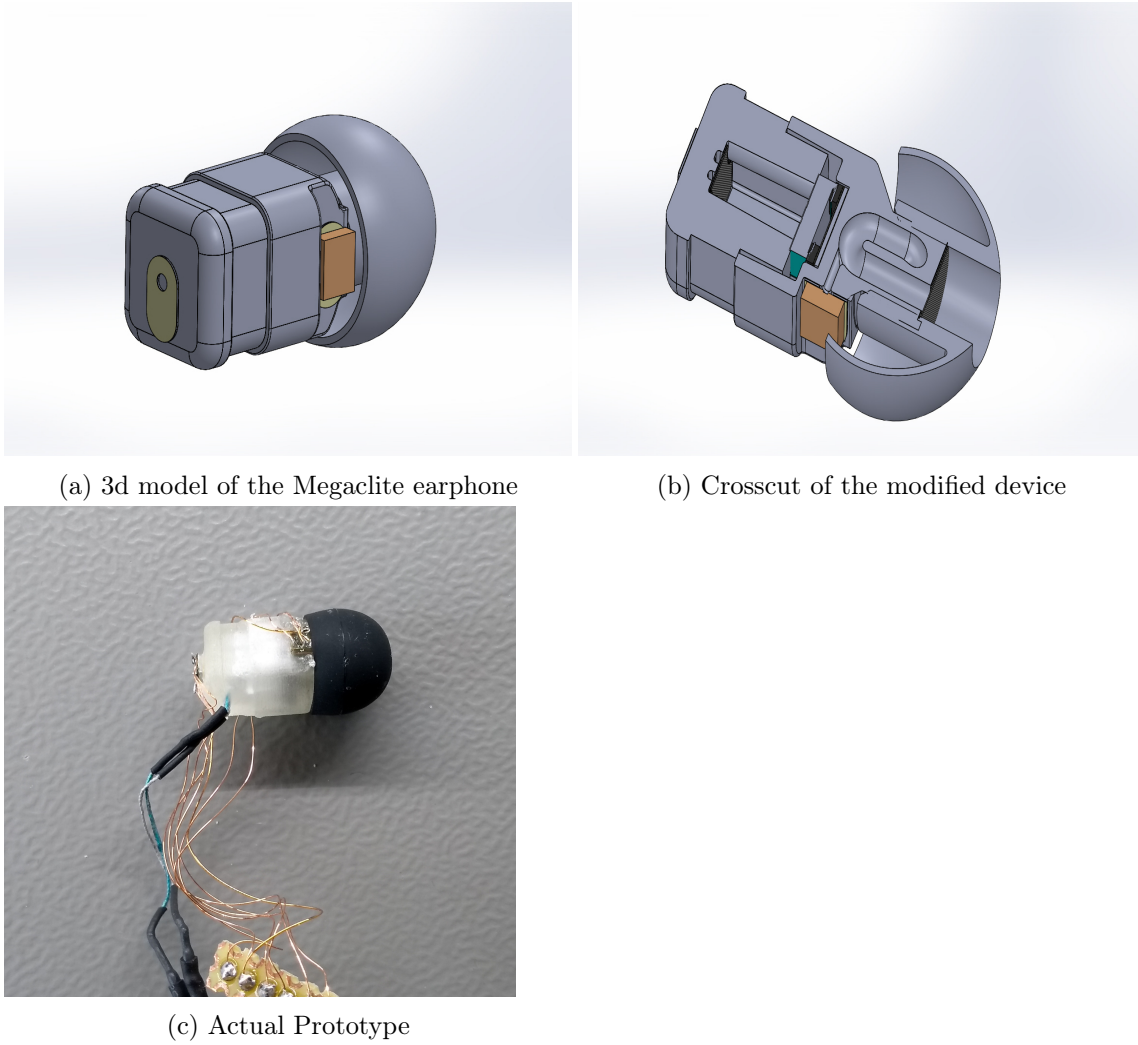


Figure 4.8: Feedback ANC prototype earphone

filter can be calculated according to equations 4.1 and 4.2.

$$A_{filter} = A_{fb} \cdot (-1) [dB] \quad (4.1)$$

$$\varphi_{filter} = \varphi_{fb} \cdot (-1) [deg] \quad (4.2)$$

where  $A_{fb}$  is the magnitude response of the feedback microphone and  $\varphi_{fb}$  is its phase response. [32]

The measured frequency responses for this prototype are shown in figure 4.10a and figure 4.10b. The red curve corresponds to the signal from the acoustic coupler and the blue curve to the signal of the feedback microphone.

The magnitude response of the feedback microphone shows a strong damping of about

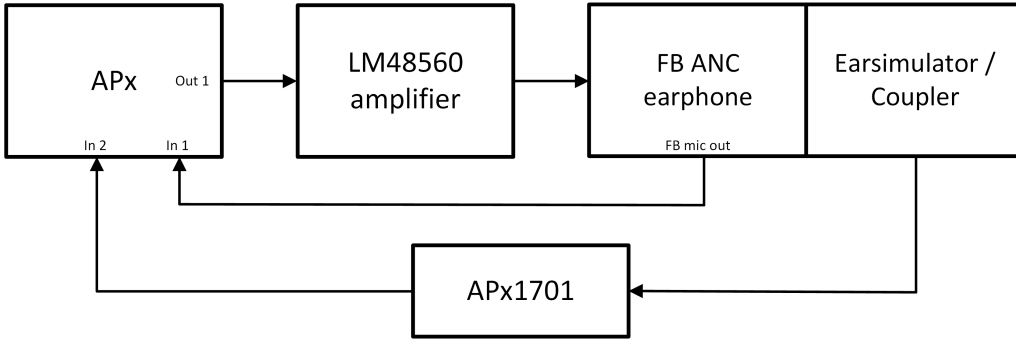
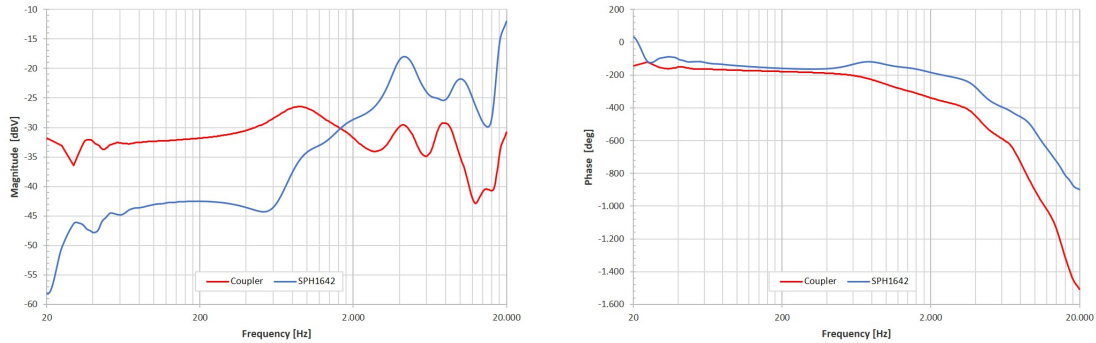


Figure 4.9: Measurement setup for the characterization of the feedback system



(a) Magnitude response

(b) Phase response

Figure 4.10: Characterization measurement results for the feedback system with SPH1642 MEMS microphone

20 dB below 2 kHz compared to the one of the reference microphone in the coupler. This turns out to be problematic for later filter design and needs to be improved.

### 4.6.3 Adjustments

#### Microphone Variation

Experiments with different types of feedback microphones were done to see if the magnitude response would improve. The MO034402-3 from DB Unlimited [33], an ECM featuring a lower cutoff frequency of 40 Hz and the ICS40619 from TDK [34], a MEMS microphone with a lower cutoff frequency of 50 Hz and differential output were used. The curves in figure 4.11 show the calculated differences between the measured magnitude responses of the feedback microphones and the acoustic coupler. All three curves have a very similar shape, but due to the lower output level of the MO034402-3 compared to the two MEMS microphones the gray curve is shifted down. From these results, it can be assumed that the mechanical design of the earphone causes the damping of the lower to middle frequencies and not the feedback microphones themselves.

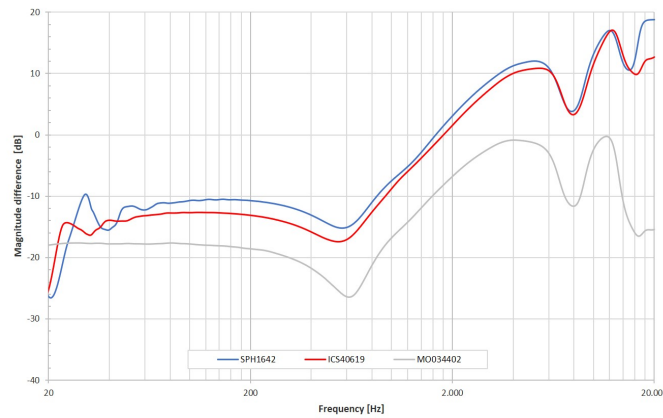


Figure 4.11: Deviation of the magnitude response of the FB microphones from the magnitude response of the acoustic coupler

### Increase of Vent Diameter

Another idea to improve the frequency response was to drill up the vent that connects the feedback microphone inlet to the inner volume of the earphone (compare with figure 4.8b). The resulting feedback microphone frequency response was again very similar and did not show any improvement. In figure 4.12, the differences in magnitude response of feedback microphone and acoustic coupler depending on the vent size are plotted.

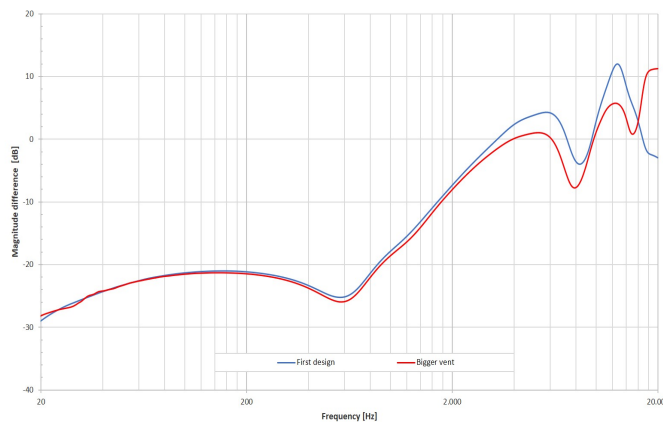


Figure 4.12: Change in magnitude response when increasing the vent diameter

Another problematic property of the feedback prototype is the strong change in magnitude response when the earphone opening is blocked. Figure 4.13 shows the measured magnitude response of the earphone.

- Blue curve: earphone in the acoustic coupler (open ear canal)
- Red curve: earphone outlet is blocked (blocked ear canal)

A difference of up to 25 dB was measured. This could potentially cause the system to become unstable when the earphone outlet is blocked by a finger, for example.

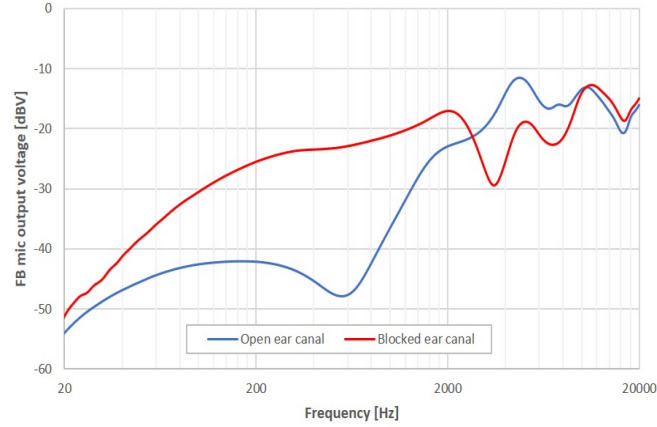


Figure 4.13: Change in magnitude response when the ear canal is blocked

Since the mechanical design of the demonstrator proved to be suboptimal for the implementation of a feedback ANC system, this approach was no longer pursued. The decision was made to switch to a feedforward topology.

## 4.7 Feedforward System

### 4.7.1 The Prototype

The Megaclite earphones that have been used for the evaluation of the feedback architecture have been reused for this investigation. The feedback microphone was removed and the underlying vent was sealed with hot glue. Then, microphones for the recording of the surrounding noise have been mounted on the backside of the earphone. The yellow pad in figure 4.8a indicates the position of the feedforward microphone on the earphone.

For the feedforward prototype, the suitability of different microphone types is also evaluated. The left earphone will be using a MEMS microphone and the right earphone will use an electret condenser microphone. As MEMS microphone the INMP510 from InvenSense, a bottom port device with a lower cutoff frequency of 60 Hz is used [35]. For the electret condenser microphone, the EM288Z1 from Primo with a lower cutoff frequency of 30 Hz is used [36]. Tables 7.1 and 7.2 in the appendix give a more detailed description of these devices and also list comparable microphones.

### 4.7.2 Earphone Characterization

Characterizing a headset is a bit more involved for a feedforward system. Figure 4.14 shows such a system and indicates the primary ( $A_1, \varphi_1$ ) and secondary ( $A_2, \varphi_2, A_{filter}, \varphi_{filter}$  and

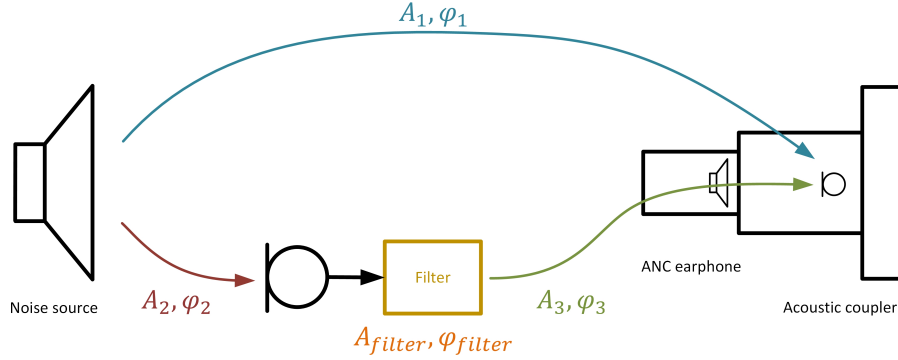


Figure 4.14: Characterization of a FF ANC system

$A_3, \varphi_3$ ) path. In order to be able to calculate the target ANC filter response, the unknown characteristics have first to be determined by measurements of:

- 1: Passive attenuation ( $A_1, \varphi_1$ )
- 2: Feedforward microphone response ( $A_2, \varphi_2$ )
- 3: Frequency response of the internal speaker ( $A_3, \varphi_3$ )

In an ideal world, the upper branch ( $A_1, \varphi_1$ ) and the lower branch ( $A_2, \varphi_2, A_{filter}, \varphi_{filter}$  and  $A_3, \varphi_3$ ) in figure 4.14 would have the exact same magnitude response but opposite phase response, as described by equations 4.3 and 4.4. The ambient noise would be canceled out completely. In reality, however, this ideal situation has to be approximated by a good filter design for the frequency band of interest.

$$A_1(f) = A_2(f) + A_{filter}(f) + A_3(f)[dB] \quad (4.3)$$

$A_{filter}(f)$  is the gain of the ideal target ANC filter,  $A_1(f)$  is the gain of the first characterization measurement,  $A_2(f)$  is the gain of the second characterization measurement and  $A_3(f)$  is the gain of the third characterization measurement. [37]

$$\varphi_1(f) = \varphi_2(f) + \varphi_{filter}(f) + \varphi_3(f) + 180^\circ[deg] \quad (4.4)$$

$\varphi_{filter}(f)$  is the phase of the ideal target ANC filter,  $\varphi_1(f)$  is the phase of the first characterization measurement,  $\varphi_2(f)$  is the phase of the second characterization measurement and  $\varphi_3(f)$  is the phase of the third characterization measurement.

The magnitude and phase response of the ideal filter can be calculated according to equations 4.5 and 4.6.

$$A_{filter}(f) = A_1(f) - (A_2(f) + A_3(f))[dB] \quad (4.5)$$

$$\varphi_{filter}(f) = \varphi_1(f) - (\varphi_2(f) + \varphi_3(f) + 180^\circ)[deg] \quad (4.6)$$

Ideally, these measurements take place in an acoustically optimized room or an anechoic chamber, but due to the fact that such a facility was not available the measurements had to be done in an ordinary room.

To overcome the issue of reverberation and the effect of room modes, the earphone was characterized in the near field of two electrodynamic speakers. Two speakers with different dimensions (7" and 2.5" diameter) had to be used to cover the frequency range up to roughly 3 kHz. The SPL, that is produced by the speakers at about 1 cm in front of the membrane, was measured using a *Beyerdynamic MM1* reference microphone and is depicted in figure 4.15. It can be seen that the 7" speaker produces more SPL in the low frequency range and is relatively linear up to approximately 700 Hz. The smaller 2.5" speaker, on the other hand, behaves linearly for frequencies between 200 Hz and 3 kHz. Hence, for each characterization step, two measurements will be done, one in the near field of the 7" speaker for the low frequencies up to 300 Hz and a second one for the mid to high frequencies using the 2.5" speaker.

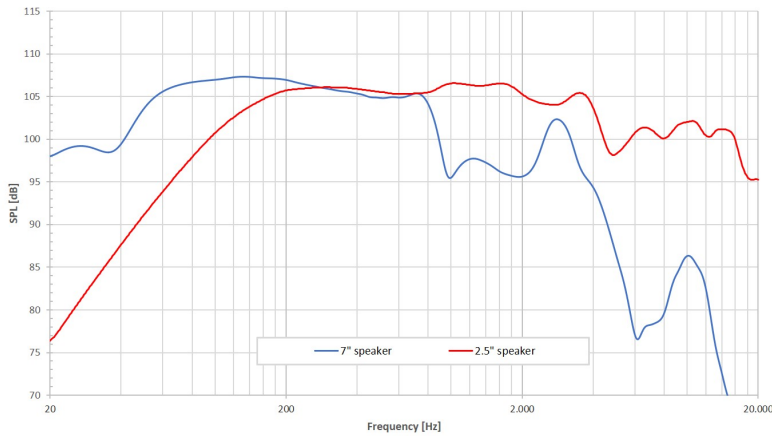


Figure 4.15: SPL measurement in the near field of the loudspeakers

The first characterization step is the measurement of the passive attenuation of the earphone. The passive attenuation quantifies the amount of ambient noise level reduction due to the wearing of the earphone. For this measurement, the earphone is plugged into the acoustic coupler, which in turn is positioned on-axis and approximately 1 cm away from the membrane of the electrodynamic speaker. Figure 4.16a shows a block diagram of the measurement setup. To properly drive the electrodynamic speaker and to provide the appropriate microphone supplies for the acoustic coupler and the reference microphone, the APx1701 transducer test interface was used [19]. The loudspeaker reproduces a sine sweep over the range of 20 Hz to 20 kHz. This signal gets damped by the earphone, is recorded by the microphone in the acoustic coupler and fed to the input of the APx system.

As mentioned above, the passive attenuation is measured for each of the two speakers. The measurement setup is shown in figure 4.17. A calibrated reference microphone is used to measure the sound pressure in the vicinity of the feedforward microphone.

The second step that needs to be done is the measurement of the feedforward microphone

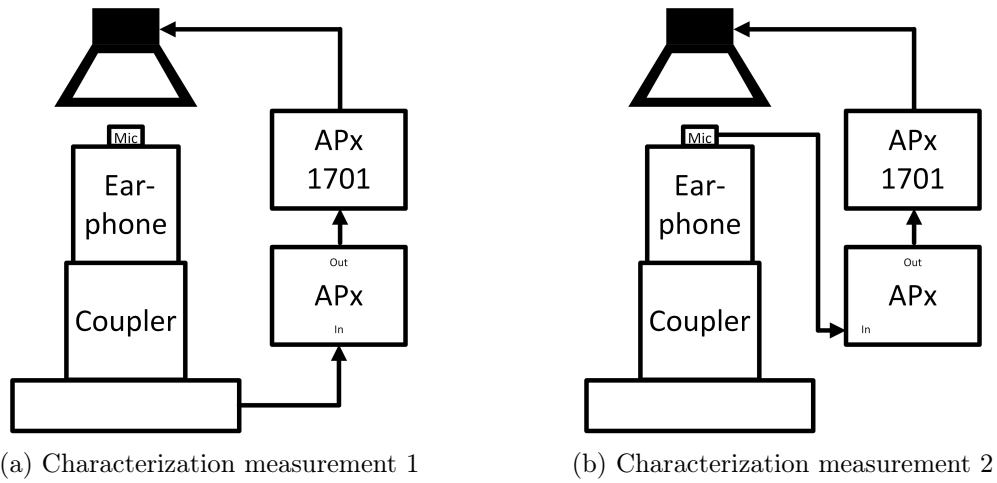


Figure 4.16: Measurement setups for characterization measurements 1 and 2

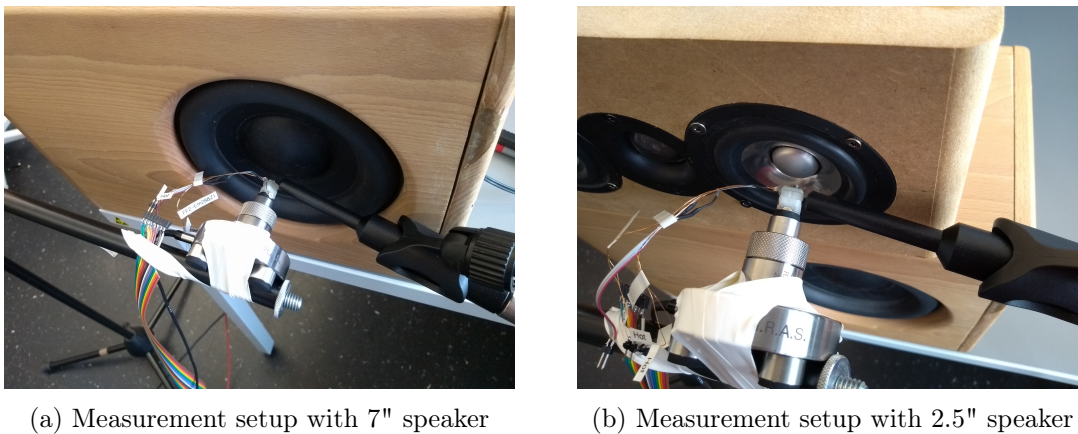


Figure 4.17: Measurements are performed in the near field of electrodynamic speakers

response. The setup is similar to the one before, but this time the signal of the feedforward microphone is passed to the APx instead of the signal from the coupler. It is depicted in figure 4.16b.

The final characterization measurement is done to obtain the frequency response of the speaker inside the earphone. The earphone is connected to the Ananke board amplifier and is then placed in the acoustic coupler. Again, a sine sweep from 20 Hz to 20 kHz is produced by the APx and the signal is routed through the AS3435 evaluation board and the LM48560 amplifier to the MEMS speaker. The microphone in the acoustic coupler records the signal coming from the earphone and passes it on to the input of the APx system. The setup is shown in figure 4.18.

From these measured frequency responses, the ideal feedforward ANC filter can be calculated with aid of equation 4.5 and equation 4.6. The APx software allows to export the measurement results in a number of different formats: *.xls*, *.xlsx*, *.csv* and *.mat*. The *.xls*

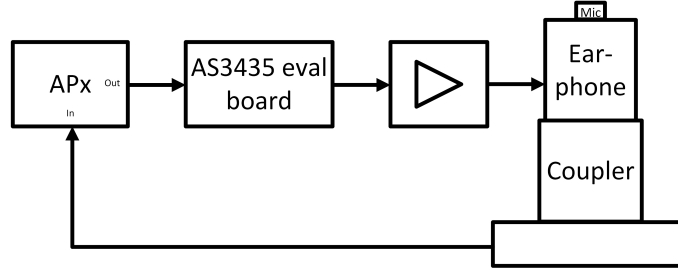


Figure 4.18: Measurement setup for characterization measurement 3

format was chosen so that the whole filter calculation could be done in Microsoft<sup>®</sup> Excel.

### 4.7.3 Filter Design

After the target filter response has been calculated, an active analog filter has to be designed that closely matches both magnitude and phase response of the target filter. Based on the equations stated in section 2.4, the filter design was done in the free SPICE simulator tool LTspice<sup>®</sup>. After simulation, the filter curves have been imported to Microsoft<sup>®</sup> Excel where the magnitude and phase response of the simulated filter could be compared to the target filter. After several iterations, the simulated filters matched closely enough for first evaluations in hardware.

#### Left Channel - MEMS Prototype

A good approximation of the determined ideal filter is critical for good ANC performance. The challenges in the filter design stem from the need to match gain and phase at the same time. In figure 4.19 the matching of the designed filter and the measured targeted filter for the left channel of the prototype is shown. As can be seen from the target filter curve, it becomes impossible to match the phase at higher frequencies which is also the reason for the bandwidth limitation of ANC. In regions where the phase difference is in the area of  $180^\circ$ , the gain of the ANC filter must be as low as possible to minimize the effect of noise amplification.

The schematic of the ANC filter for the left channel is depicted in figure 4.20.

It consists of a high pass filter at the input, a non-inverting amplifier, two notch filters and an active low pass filter. The high pass filter formed by C60 and R86 has a cutoff frequency of 3.3 Hz (equation 4.7) and is used to remove any DC offset coming from the microphone.

$$f_{HPF_{3dB}} = \frac{1}{2\pi RC} = \frac{1}{2\pi \cdot 22 k\Omega \cdot 2.2 \mu F} = 3.3 Hz \quad (4.7)$$

The non-inverting amplifier is integrated in the AS3435 and can be set via the provided software to adjust the microphone gain. For the left channel, the microphone gain is set

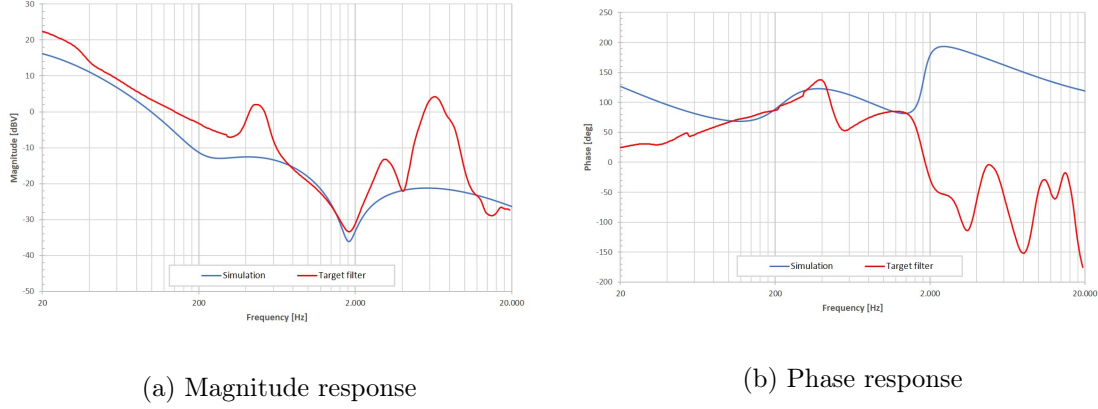


Figure 4.19: Frequency response of designed filter versus target filter for the left channel

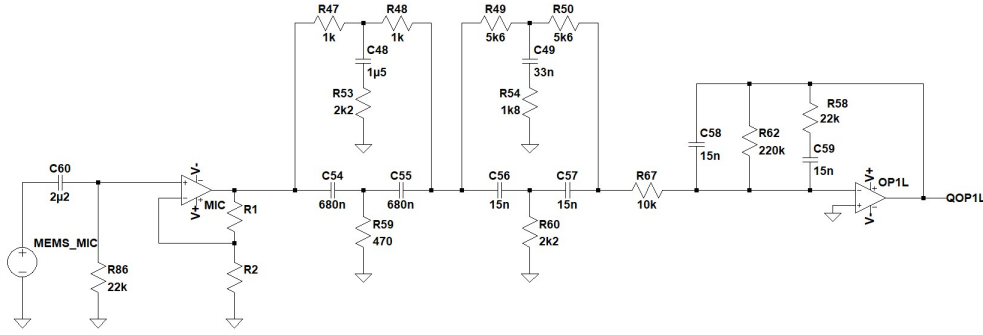


Figure 4.20: Filter for left channel using a MEMS microphone for ANC

to 0 dB. The two twin-T notch filters have their notch frequencies at 234.1 Hz and 1895 Hz according to equations 4.8 and 4.9.

$$f_{notch1} = \frac{1}{2\pi RC} = \frac{1}{2\pi \cdot 1 \text{ k}\Omega \cdot 680 \text{ nF}} = 234.1 \text{ Hz} \quad (4.8)$$

$$f_{notch2} = \frac{1}{2\pi RC} = \frac{1}{2\pi \cdot 5.6 \text{ k}\Omega \cdot 15 \text{ nF}} = 1895 \text{ Hz} \quad (4.9)$$

The final stage is an operational amplifier in inverting configuration that forms an active low pass filter. If  $R58$  and  $C59$  are not in place, the parameters for the low pass filter can be calculated:

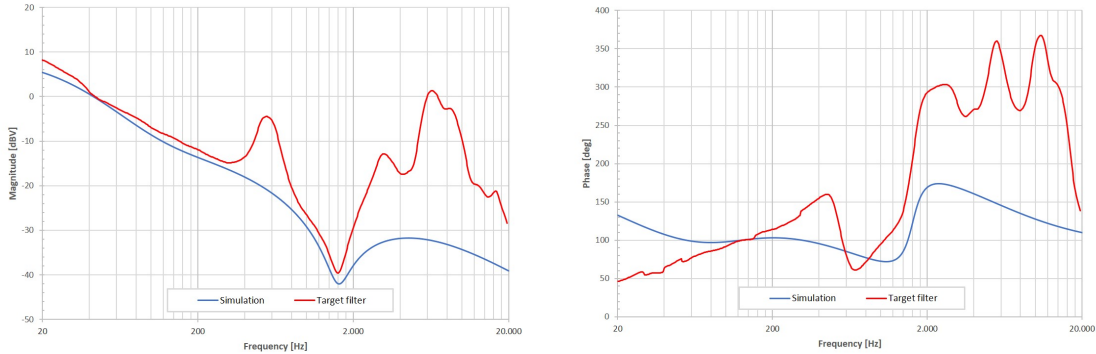
$$A_{LPF_{dB}} = 20 \cdot \log\left(\frac{R_{62}}{R_{67}}\right) = 20 \cdot \log\left(\frac{220 \text{ k}\Omega}{10 \text{ k}\Omega}\right) = 26.85 \text{ dB} \quad (4.10)$$

$$f_{LPF_{3dB}} = \frac{1}{2\pi \cdot R_{62} \cdot C_{58}} = \frac{1}{2\pi \cdot 220 \text{ k}\Omega \cdot 15 \text{ nF}} = 48.2 \text{ Hz} \quad (4.11)$$

The additional parallel feedback path formed by R58 and C59 increases the phase in the region around 1 kHz and reduces the gain for low frequencies. The component values have been found by simulation. The MEMS microphone is supplied with  $2.7 V_{typ}$  via the integrated microphone supply pin MICS of the AS3435.

### Right Channel - ECM Prototype

The target filter for the right channel is quite similar to the one required for the left channel. Figure 4.21 shows the calculated target filter response as well as the designed filter response. It can be seen that the simulated filter matches the ideal filter quite well in the range of 60 Hz to 1.6 kHz.



(a) Magnitude response

(b) Phase response

Figure 4.21: Frequency response of designed filter versus ideal filter

The ANC filter for the right channel is depicted in figure 4.22. It uses the same topology as the filter for the left channel but some component values have been changed to reach the desired filter response. Again, there is a 3.3 Hz high pass filter at the input for AC coupling the microphone signal followed by the AS3435s internal microphone preamplifier. The notch frequencies of the two twin-T notch filters are set at 120 Hz and 1.6 kHz. The final stage is, again, an inverting low pass filter with additional parallel feedback path formed by R102 and C94. The electret microphone is supplied via the AS3435's integrated microphone charge pump. A  $15 k\Omega$  bias resistor is used as suggested in the EM288Z1 datasheet [36].

## 4.8 Implementation

After the filter design for the two channels was done, the ANC filters were implemented on the AS3435 evaluation board by soldering the corresponding components on the board. In figure 4.23 the setup is depicted. The left side shows the USound Ananke board that is used to drive the MEMS speaker. On the right hand side, the AS3435 evaluation is shown.

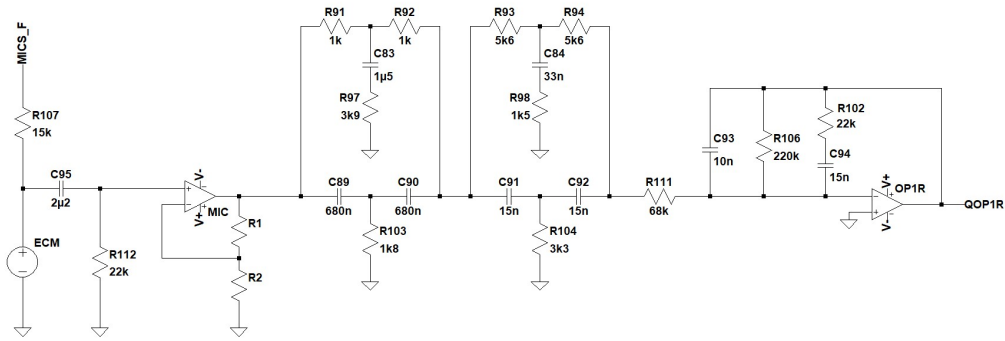


Figure 4.22: Filter for right channel using an ECM microphone for ANC

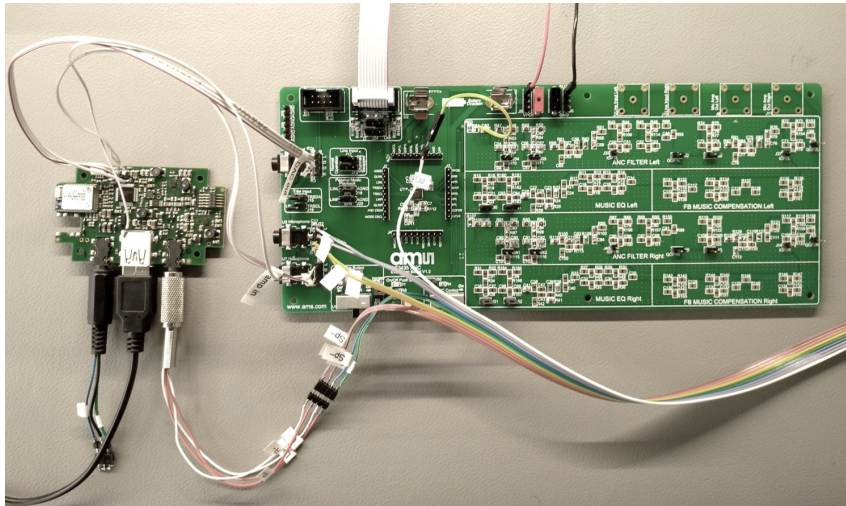


Figure 4.23: AS3435 evaluation board with ANC filters for the feedforward prototype

## 4.9 Measurement of Performance of the 1st FF System

The performance of an ANC headphone can be evaluated by measuring the passive attenuation and comparing it with the active attenuation when the ANC circuitry is turned on. To measure this, the earphone is placed in the acoustic coupler and a sine sweep in the range of 20 Hz to 20 kHz is being played back. A block diagram of the measurement setup is shown in figure 4.24. The electrodynamic speaker is driven by the APx1701 transducer interface, the Ananke board is used to drive the MEMS speaker in the earphone. For the performance analysis of the prototype, the measurements were conducted in the near field of the electrodynamic speakers.

### 4.9.1 Feedforward System Left Channel

The blue curve in figure 4.25 shows the signal picked up by the acoustic coupler for the left earphone when the ANC functionality is turned off. The red curve shows the result of the

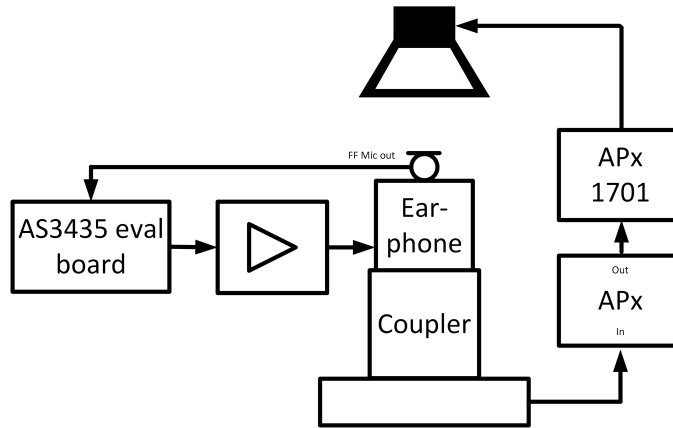


Figure 4.24: Block diagram for ANC performance measurements

same measurement, but this time with the ANC functionality turned on. The area between the two curves corresponds to the ANC performance at 110 dB SPL. Noise cancellation is achieved, when the red curve is lower than the blue curve, which is mainly the case for frequencies between 60 Hz and 800 Hz. At 160 Hz, the peak performance of roughly 17 dB in noise reduction is achieved. In regions where the red curve is above the blue curve, the ambient noise is actually being amplified as for frequencies lower than 60 Hz, for example. Further optimization on the ANC filter is necessary to reduce these areas.

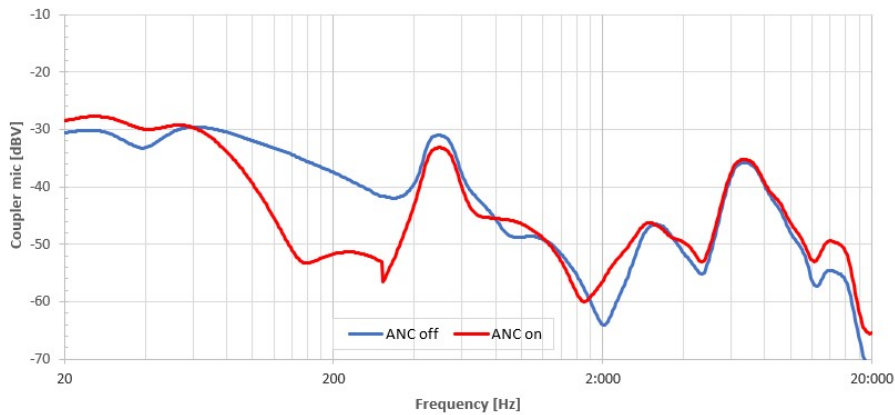


Figure 4.25: Measured ANC performance of left channel at 110 dB SPL

#### 4.9.2 Feedforward System Right Channel

The measured ANC performance for the right channel of the prototype that uses an electret condenser microphone is shown in figure 4.26. Again, the measurements were conducted at 110 dB SPL. It can be seen that noise reduction is achieved over the whole band up to 1.5 kHz. A noise reduction of about 16 dB is achieved at 90 Hz. From 1.5 kHz up to 3 kHz, the noise is again amplified with a maximum amplification of 3 dB at 1.8 kHz.

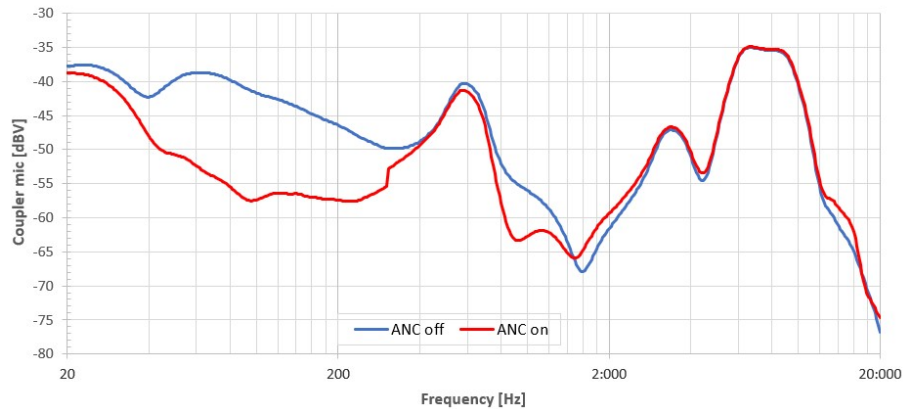


Figure 4.26: Measured ANC performance of right channel at 110 dB SPL

### 4.9.3 Adjustments

After analyzing the ANC performance of the prototype, it became apparent that both channels had a very low performance in the band between 400 Hz and 800 Hz. The passive attenuation in this band is also remarkably low. To find the root cause of this, more passive attenuation measurements with different shaped eartips used on the prototypes have been done. The used eartips are shown in figure 4.27.



Figure 4.27: Different types of eartips that have been investigated. From left to right: black, red, transparent black

The measured passive attenuation for one and the same earphone with different eartips is depicted in figure 4.28a. The measurements have been done in the near field of the 2.5 " speaker. The blue curve represents the SPL in close proximity to the earphone measured by a reference microphone, the remaining curves show the SPL measured by the acoustic coupler and correspond to the passive attenuation of the earphone when different eartips are used. As can be seen, the frequency and the amplitude of the notch in attenuation varies with the chosen eartip.

The measurement of passive attenuation showed a significant variation for the different eartips. Furthermore, an additional deviation of the results when repeating the measurements was observed. This was mainly caused by a varying insertion depth of the earphone in the acoustic coupler. To ensure reproducible results, the earphone was then fixed to the

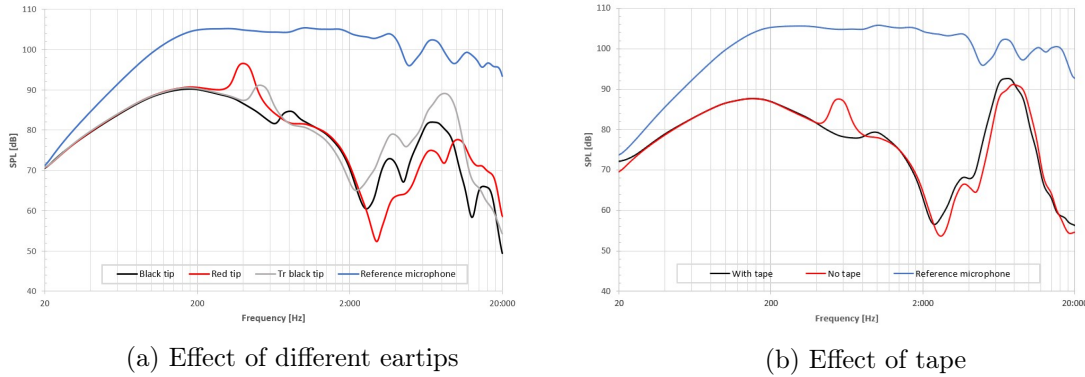


Figure 4.28: Passive attenuation measurement results

acoustic coupler using adhesive tape as shown in figure 4.30b. This resulted in a complete disappearance of the notch in passive attenuation as can be seen in figure 4.28b. This suggests that the notch in the attenuation measurements was caused by mechanical vibrations of the earphone in the acoustic coupler.

To evaluate the effect of the improved passive attenuation on the required target filter, a recharacterization on the left earphone of the prototype was done. In figure 4.29, the magnitude and phase response of the new target filter as well as the previously designed ANC filter are shown. As expected, the peak in magnitude and phase response around 400 Hz disappeared. Since the matching between the two filter responses is not optimal, a filter redesign is necessary.

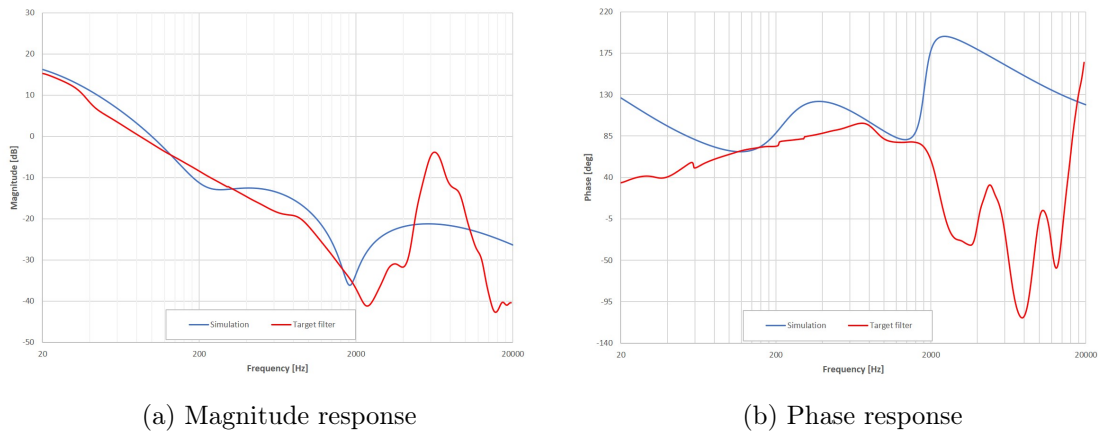
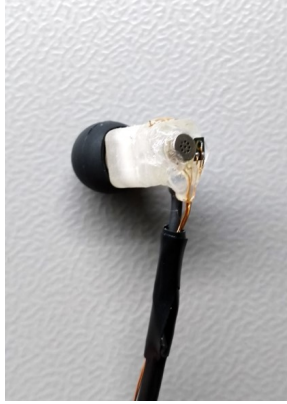


Figure 4.29: Frequency response of previously designed filter versus ideal filter after re-characterization

## 4.10 Recharacterization and Redesign

To allow a better comparison of the influence of the microphones, the right earphone was modified. Both a MEMS and an electret microphone have been glued to the backside of the earphone as shown in figure 4.30a. Two separate earphone characterizations were done, one using the INMP510 MEMS microphone and a second one using the EM288Z1 electret microphone as feedforward microphone.



(a) Prototype with MEMS and electret microphone



(b) Earphone taped to coupler

Figure 4.30: Prototype earphone used for the recharacterization measurements

### 4.10.1 Left Channel - MEMS Microphone

The new magnitude and phase responses of the target filter and the redesigned ANC filter, when the MEMS microphone is used are shown in figure 4.31. The designed filter matches the magnitude response quite well from 40 Hz to approximately 2 kHz. The phase response, on the other hand, could not be matched precisely. The phase of the target filter is rising at low frequencies. This is due to the fact that the INMP510 only has a lower 3 dB corner frequency of 60 Hz.

The updated schematic of the ANC filter for the left channel is depicted in figure 4.32.

As before, the high pass filter for the MEMS microphone is set to 3.3 Hz:

$$f_{HPF_{3dB}} = \frac{1}{2\pi RC} = \frac{1}{2\pi \cdot 22 \text{ k}\Omega \cdot 2.2 \text{ }\mu\text{F}} = 3.3 \text{ Hz} \quad (4.12)$$

The microphone preamplifier gain is set to 10 dB via the AS3435 configuration software. The following notch filter stage is tuned to a frequency of 2.4 kHz according to equation 4.13.

$$f_{notch} = \frac{1}{2\pi RC} = \frac{1}{2\pi \cdot 5.1 \text{ k}\Omega \cdot 13 \text{ nF}} = 2.4 \text{ kHz} \quad (4.13)$$

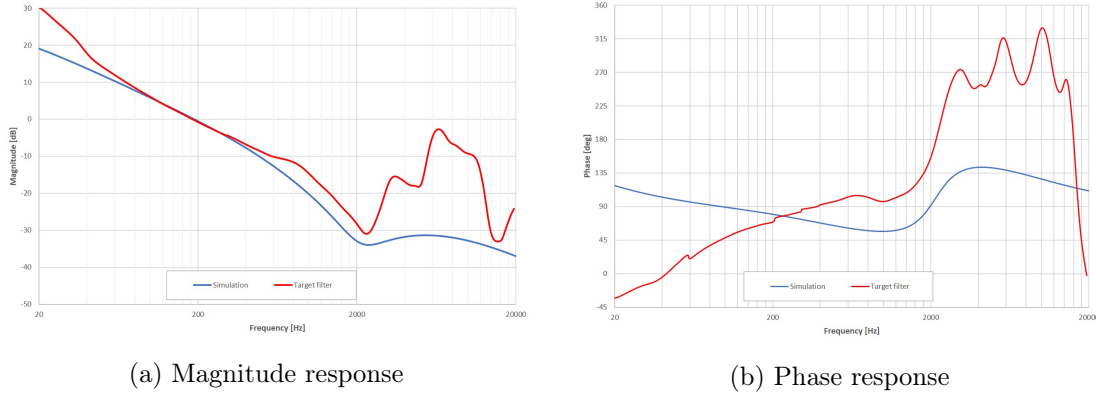


Figure 4.31: Frequency response of designed filter versus ideal filter - MEMS microphone

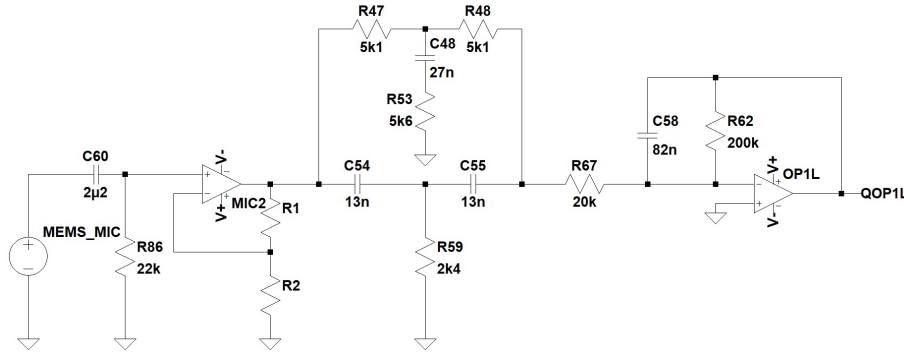


Figure 4.32: Schematic of the redesigned ANC filter with MEMS feedforward microphone

As the final stage, an active inverting low pass filter is implemented.

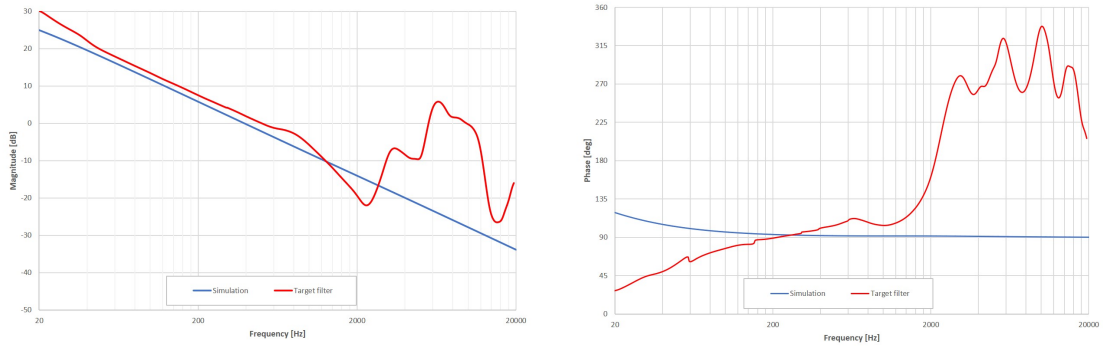
$$A_{LP_{dB}} = 20 \log \left( \frac{R62}{R67} \right) = 20 \log \left( \frac{200 \text{ k}\Omega}{20 \text{ k}\Omega} \right) = 20 \text{ dB} \quad (4.14)$$

$$f_{LP_{3dB}} = \frac{1}{2\pi \cdot R62 \cdot C58} = \frac{1}{2\pi \cdot 200 \text{ k}\Omega \cdot 82 \text{ nF}} = 9.7 \text{ Hz} \quad (4.15)$$

#### 4.10.2 Right Channel - Electret Microphone

When the electret microphone is used, the overall target filter response remains similar to the one where the MEMS microphone is used. Figure 4.33 depicts the frequency response of the target filter and the designed ANC filter. Due to the fact that the Primo EM288Z1 has a lower 3 dB corner frequency, compared to its MEMS counterpart, less gain is needed at the low frequencies. Also, the phase response is flatter, which makes it easier to approximate with the ANC filter. It can be seen that the gain is about 1.5 dB too low for the lower frequencies. This is a trade-off between noise cancellation performance at lower

frequencies and noise amplification around 2 kHz and can easily be adjusted by increasing the microphone gain later on.



(a) Magnitude response

(b) Phase response

Figure 4.33: Frequency response of designed filter versus ideal filter - electret microphone

The schematic of the designed ANC filter is shown in figure 4.34. It is basically the same filter as the previous one, except that it does not include a notch filter and that the preamplifier gain is set to 12.5 dB.

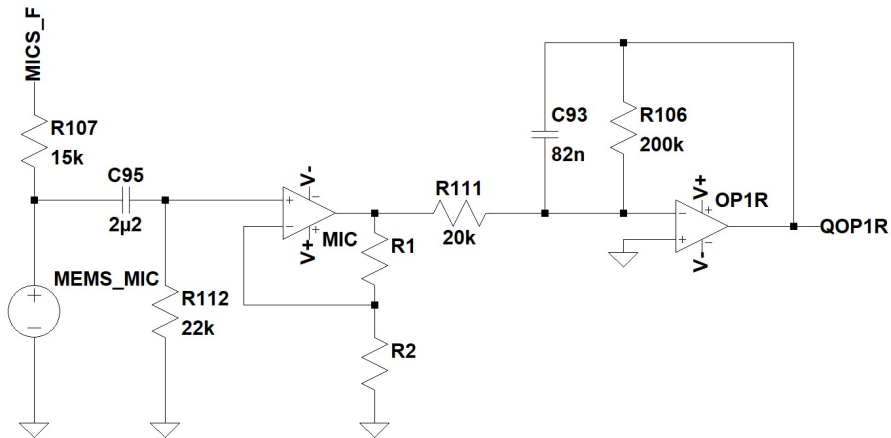


Figure 4.34: Schematic of the redesigned ANC filter - electret microphone

## 4.11 Measurement of Performance of the 2nd FF System

Figure 4.35 shows the measured passive and active attenuation of the recharacterized system. The blue curve represents the passive attenuation of the earphone, the red and green curves are the active attenuation when the ANC is turned on for the left and right channel. The performance has clearly improved compared to the first prototype, especially in the region from 300 Hz to 1800 Hz. The peak in noise reduction for the left channel is reached at approximately 230 Hz, which is the frequency where the designed filter has the exact same phase response as the target filter. The active attenuation significantly improves at lower frequencies when the ECM is used instead of the MEMS microphone. This is due to the better low frequency behavior of the electret microphone.

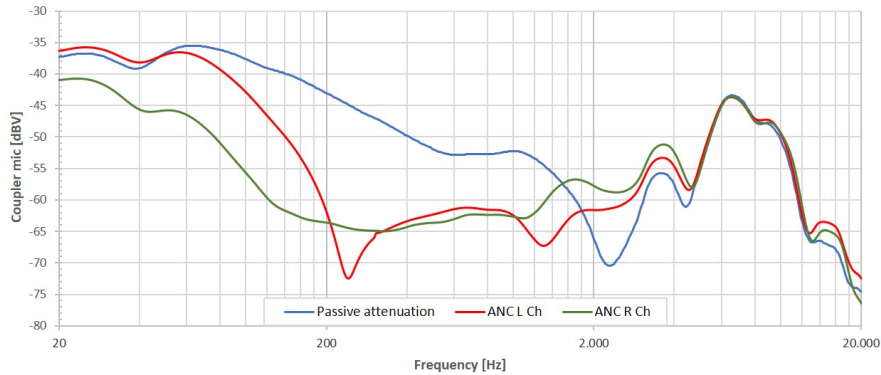


Figure 4.35: Passive attenuation vs active attenuation of the recharacterized system at 106 dB SPL

## 4.12 Subjective Evaluation

After the implementation of the recharacterized system, a subjective listening test was performed. For this, a test person wearing the ANC earphones was sitting 1 meter in front of a loudspeaker that was playing white noise. First, the ANC was deactivated to accustom the test person to the passive attenuation of the earphones. Then, the ANC functionality was turned on and the difference in attenuation was judged by the test person. Surprisingly, the subjective ANC performance was rated quite low but improved considerably when the gain of the feedforward microphone was increased. This indicates that in the real life wearing situation, there is more leakage between earphone and ear canal than there is in the system used for the characterization of the earphone. The fitting of the eartip to the acoustic coupler is rather tight and does not change during the characterization measurements, whereas in the actual use case the fitting will change. This impacts the passive attenuation of the earphone and thus also alters the desired frequency response of the required ANC filter.

### 4.13 Effect of Leakage

The effect of leakage on the ANC performance of the demonstrator was investigated further by deliberately introducing additional leakage between the earphone and the acoustic coupler. This was done by placing short pieces of wire with varying diameters between eartip and coupler as shown in figure 4.36. To simulate a small leakage, a wire diameter of 0.21 mm was used. For introducing a big leakage, a wire diameter of 0.4 mm was used.



Figure 4.36: Leakage is simulated by placing wire between coupler and eartip

#### 4.13.1 MEMS Speaker Response

As generally with in-ear headphones, the bass response of the Megaclite earphones is largely dependent on a tight wearing situation. In figure 4.37, the internal speaker response of the Megaclite earphones for three different wearing scenarios is shown: tight fit, small leakage and big leakage. It can be seen that the small leakage reduces the SPL at 20 Hz by about 2 dB. When the wire with 0.4 mm diameter is used to introduce a big leakage, the bass response at 20 Hz drops by roughly 11.5 dB.

#### 4.13.2 Passive Attenuation

As expected, the passive attenuation of the earphone is reduced by introducing additional leakage. Figure 4.38 shows the measured change in passive attenuation from a tight fit to a wearing situation with leakage. The blue curve shows the reduction in passive attenuation when a small leak (using a wire diameter 0.21 mm) is present, the red curve shows the change with a big leak (0.4 mm wire diameter). A small leakage already leads to a decrease of about 8.5 dB at 100 Hz. For this measurement, the earphone was not taped to the acoustic coupler and therefore the graph shows the characteristic peaks between 600 Hz and 800 Hz.

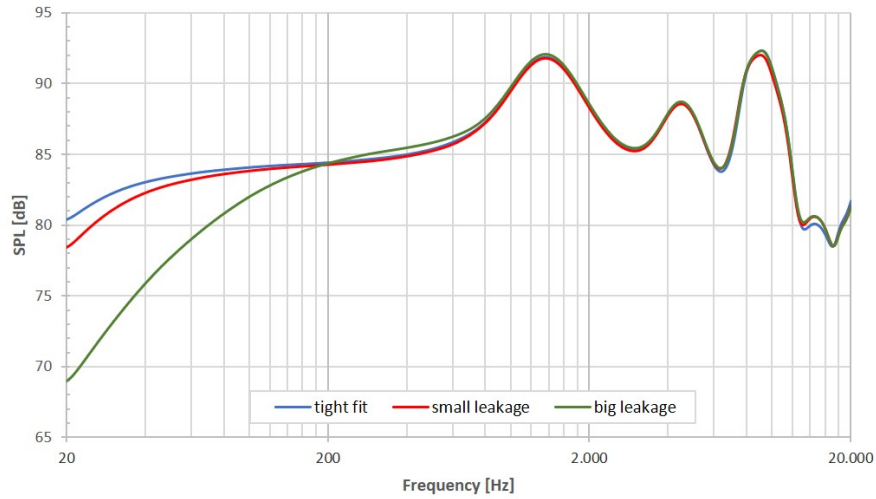


Figure 4.37: Loss of bass response with increased leakage

### 4.13.3 ANC Performance

Finally, the effect of a leaky wearing situation on the ANC performance of the demonstrator was measured and is shown in figure 4.39. The blue curve is the ANC performance of the right channel of the demonstrator when the earphone sits tightly in the acoustic coupler. The red and green curves show the ANC performance when a leakage is present. These measurement results confirm the subjective test results and indicate that the root cause is the increased leakage between eartip and acoustic coupler. The biggest loss of performance is observed in the lower frequency range, which is also the region where the passive attenuation changed the most.

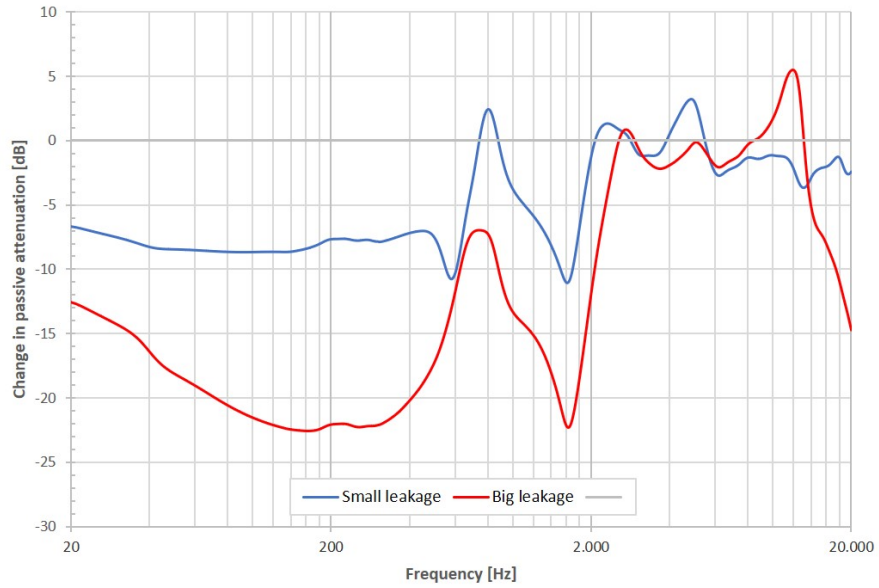


Figure 4.38: Reduction in passive attenuation due to increased leakage

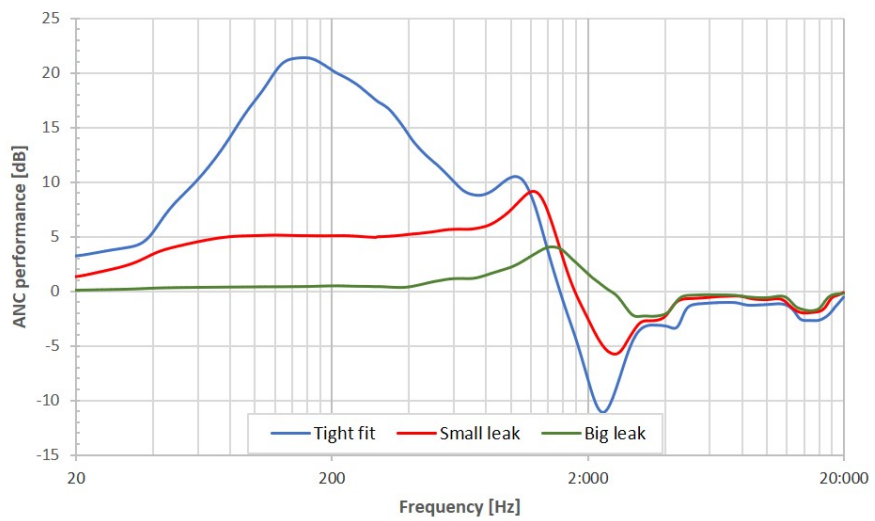


Figure 4.39: Reduction in ANC performance due to increased leakage

## Chapter 5

# Results and Discussion

### 5.1 Feedback System

The intended implementation of a feedback system was no longer pursued after evaluating the results of the characterization measurements. As shown in figure 4.11, the main problem is the strong damping of the feedback microphone signal for frequencies below 2 kHz. The use of various feedback microphones (both MEMS and electret) for the demonstrator has been evaluated and in every case a similar frequency response could be observed. This indicates that the damping results from the mechanical design of the earphone. Furthermore, the big change in the frequency response of the feedback microphone, when the earphone is blocked, is challenging for a stable implementation. A redesign of the in-ear headphone that allows the feedback microphone to be located inside the earphone is advised for further investigation.

### 5.2 Feedforward System

After recharacterizing and adjusting the feedforward system, it shows clear improvements to the first version. The measured ANC performance for tight fitting earphones, shown in figure 5.1, suggests a better suitability of electret microphones (right channel) over MEMS microphones (left channel). This is mainly due to the fact that electret microphones with lower -3 dB corner frequencies are available compared to their counterparts. Also, the ANC performance is more stable over the low to medium frequency range and does not show any significant performance peaks. A noise reduction is achieved for frequencies up to 1.6 kHz with a peak performance of 21 dB between 140 Hz and 160 Hz. Above 1600 Hz, noise is added to the speakers with the region between 1.6 kHz and 3 kHz being the most problematic one. The noise amplification in this region stems from the frequency response mismatch of the ANC filter to the target filter as can be seen in figure 4.33. For the left channel, the noise amplification is less severe. The reason for this is a better matching of the frequency response of the ANC filter due to the additional notch filter at 2.4 kHz.

The observed effect of noise amplification in a certain frequency band is also reported in

[14]. The ANC performance of 13 headphones has been evaluated using pink noise as test signal. On all tested devices, a boosting of noise by about 5 dB for frequencies above 1.25 kHz has been observed. For the only in-ear headphone in the test, a boost of 9 dB at 4 kHz was measured. This is comparable to the obtained results from the ANC prototype.

When looking at the passive attenuation of the earphone used for the demonstrator, it becomes apparent that there is a peak in attenuation around 2.2 kHz (compare with figure 4.35). This is causing the ANC target filter to have a notch in its magnitude response, which is hard to match with the implemented analog filter. Therefore, the overall frequency dependence of the passive attenuation must be taken into account for a potential redesign of the earphone.

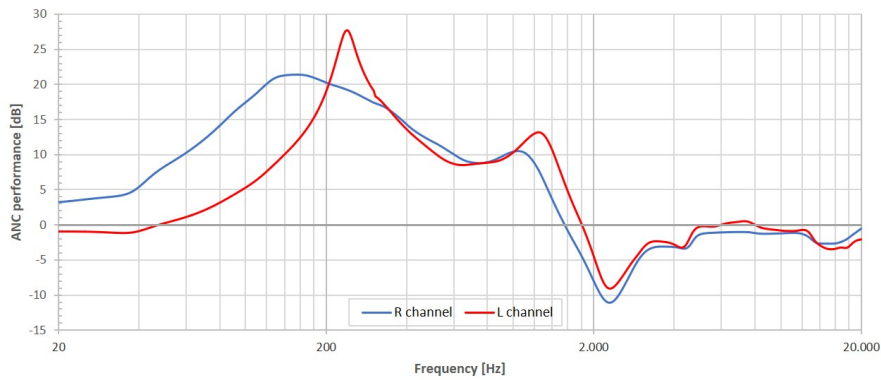


Figure 5.1: ANC performance at 106 dB SPL

The biggest impact on the ANC performance is the wearing situation of the demonstrator. While figure 5.1 suggests approximately 20 dB in noise reduction at low frequencies, figure 4.39 draws a different picture. Already a relatively small leakage reduces the ANC performance to only 5 dB in the low frequency range. It is also worth noting that the peak in noise amplification is reduced and is shifted to slightly higher frequencies.

For bigger leakages, there is almost no noise reduction taking place any more. The ANC performance shows its peak of 4 dB at approximately 1.4 kHz, whereas it is not noticeable for frequencies up to 400 Hz. The effect of noise amplification is also diminished as already observed with smaller leakages.

While increased leakage negatively impacts the low frequency response of the Megaclite earphones (compare with figure 4.37), the main reason for the strong impact on ANC performance is the big change in passive attenuation as shown in figure 4.38. The reason for this is the passive attenuation of the Megaclite earphones which is relatively high and hence even a small introduced leakage has a big influence on the sound isolation. For a potential redesign, a more open earphone should be considered so that the effect of additional leakage does not affect the passive attenuation that strongly.

On the other hand, a more open design also reduces the SPL in the earphone at low frequencies. A possibility to compensate for this would be to use two MEMS speakers in parallel combined with audio filtering to again flatten the frequency response of the earphone.

# Chapter 6

## Closure

### 6.1 Conclusions

In this work, an ANC demonstrator based on an analog off the shelf solution was developed. While the performance in an ideal wearing situation is comparable to commercial devices, it does not hold up in a realistic use case. The main performance limitation stems from the mechanical design of the used prototype earphone, which shows big changes in passive attenuation for small changes in the wearing situation. A redesign with an earphone that is more open is suggested.

The use of MEMS and electret microphones for the demonstrator has been compared and it became apparent that the electret microphones are more suitable for noise cancellation applications. This is due to the better low frequency behavior compared to the available MEMS type microphones. The downside is that the sensitivity of electret microphones is varying by  $\pm 3$  dB, while MEMS microphones can be obtained with  $\pm 1$  dB tolerance. This makes a production trimming of the ANC filter gain necessary.

#### 6.1.1 Improvements

The quality of the earphone characterization is expected to be improved when performed in an anechoic chamber due to the fact that reflections from the surroundings are minimized. Such a facility would also allow for more precise subjective listening tests to evaluate the performance of an ANC prototype.

For future characterization measurements, the use of an ear and cheek simulator is suggested to be able to model the actual wearing situation more realistically.

Also, the use of one coaxial full range loudspeaker is preferred to the use of two separate loudspeakers. This is due to the fact that the measurement results for the two loudspeakers have to be spliced together and need to be averaged in the region of overlap to obtain smooth curves. The averaging introduces slight inaccuracies and should best be avoided.

With the use of current generation MEMS speakers, a significant performance improvement can be expected. This is due to improved speaker characteristics and reduced part to part variations that have been achieved in the meantime.

## 6.2 Future Work

From the evaluation of the results, it becomes apparent that a redesign of the used earphone is a necessary next step. Using a different earphone design that enables the integration of the feedback microphone is proposed to re-evaluate the performance of a feedback system. It is expected to be less susceptible to changing leakage in a wearing situation.

Also, a separate earphone design with increased leakage hole and two MEMS speakers is proposed for the feedforward ANC evaluation. The increased leakage will diminish the effects of the wearing situation on the ANC performance, while a second speaker is proposed to account for the reduction in bass response of such an earphone.

Furthermore, new adaptive ANC solutions allowing small form factors and low power consumption have recently been introduced to the market [38]. A prototype based on an adaptive ANC system should be developed to evaluate the benefits over the static systems covered in this work.

Chapter 7

Appendix

Part	Manufacturer	SNR [dB]	Frequency [Hz]
EM288Z1	PRIMO	70	30 - 10 k
MO034402-4	DB Unlimited	60	40 - 20 k
MO034402-3	DB Unlimited	52	40 - 20 k
MO034402-2	DB Unlimited	60	40 - 20 k
MN044402-1	DB Unlimited	55	40 - 20 k
CMC-3015	CUI	56	100 - 20 k

Part	Sensitivity [dB]	Size [mm]	AOP [dBSPL]
EM288Z1	-43 $\pm$ 3	$\phi$ 4 x 2	127
MO034402-4	-44 $\pm$ ?	$\phi$ 3 x 1.5	-
MO034402-3	-44 $\pm$ ?	$\phi$ 3 x 1.2	-
MO034402-2	-44 $\pm$ ?	$\phi$ 3 x 1.2	-
MN044402-1	-44 $\pm$ 4	$\phi$ 4 x 1.5	-
CMC-3015	-44 $\pm$ 3	$\phi$ 3 x 1.5	-

Table 7.1: Electret microphones for ANC

Part	Manufacturer	SNR [dB]	Frequency [Hz]	Sensitivity [dB]
SPH0642HT5H-1	Knowles	65	100 - 10 k	-38 $\pm$ 1
SPH1642HT5H-1	Knowles	65	60 - 15 k	-38 $\pm$ 1
ICS-40181	TDK	65	60 - 20 k	-38 $\pm$ 1
ICS-40619	TDK	67	50 - 20 k	-38 $\pm$ 1
SPW0442	Knowles	59	50 - 20 k	-42 $\pm$ 1
MP23AB02B	ST	64	100 - 13 k	-38 $\pm$ 3
ICS-40180	InvenSense	65	60 - 20 k	-38 $\pm$ 1
INMP510	InvenSense	65	60 - 20 k	-38 $\pm$ 2

Part	Size [mm]	AOP [dBSPL]	Orientation
SPH0642HT5H-1	3.5 x 2.65 x 1	124	top port
SPH1642HT5H-1	3.5 x 2.65 x 1	124	top port
ICS-40181	3.5 x 2.65 x 0.98	124	top port
ICS-40619	3.5 x 2.65 x 0.98	132	top port
SPW0442	3.1 x 2.5 x 1	128	top port
MP23AB02B	3.35 x 2.5 x 0.98	124	bottom port
ICS-40180	3.5 x 2.65 x 0.98	124	bottom port
INMP510	3.5 x 2.65 x 0.98	124	bottom port

Table 7.2: MEMS microphones for ANC

# Bibliography

- [1] *USound MEMS-Speakers THD Assessment*, USound GmbH., 2020, <https://www.usound.com/download/thd-whitepaper/>, visited 24 October 2020.
- [2] *Integrated Circuits for High Performance Electret Microphones (SNAA114)*, Texas Instruments, 2011, <https://www.ti.com/lit/wp/snaa114/snaa114.pdf>, visited 24 October 2020.
- [3] *Tutorial for MEMS microphones (Application Note AN4426)*, STMicroelectronics, 2017, [https://www.st.com/resource/en/application\\_note/dm00103199-tutorial-for-mems-microphones-stmicroelectronics.pdf](https://www.st.com/resource/en/application_note/dm00103199-tutorial-for-mems-microphones-stmicroelectronics.pdf), visited 24 October 2020.
- [4] *SiSonic Design Guide (Application Note AN24)*, Knowles Acoustics, 2017, <https://www.knowles.com/docs/default-source/default-document-library/sisonic-design-guide.pdf>, visited 24 October 2020.
- [5] *MEMS Microphones for Active Noise Cancellation Applications (Application Note AN-000056)*, InvenSense Inc., 2015, <https://www.invensense.com/wp-content/uploads/2016/05/AN-000056-v1.0.pdf>, visited 24 October 2020.
- [6] *USound MEMS-Speakers Introduction*, USound GmbH., 2020, <https://www.usound.com/download/whitepaper-mems-speakers/#>, visited 24 October 2020.
- [7] *AS3415/AS3435 Integrated Active Noise Cancelling Solution with Bypass Feature*, ams AG, 2014, <https://ams.com/as3435>, visited 24 October 2020.
- [8] D. Guicking, “Patents on active control of noise and vibration - an overview,” 2009.
- [9] P. Lueg, “Process of silencing sound oscillations,” U.S. Patent 2 043 416, June 1936.
- [10] H. F. Olson and E. G. May, “Electronic sound absorber,” *The Journal of the Acoustical Society of America*, vol. 25, no. 6, pp. 1130–1136, 1953. [Online]. Available: <https://doi.org/10.1121/1.1907249>
- [11] W. B. Conover and W. F. M. Gray, “Noise reducing system for transformers,” U.S. Patent 2 776 020, January 1957.
- [12] C. Hansen, *Understanding Active Noise Cancellation*. CRC Press, 2001. [Online]. Available: <https://doi.org/10.1201/9781482267570>

- [13] D. Miljković, “Active noise control: From analog to digital - last 80 years,” 05 2016, [https://www.researchgate.net/publication/304079106\\_Active\\_Noise\\_Control\\_From\\_Analog\\_to\\_Digital\\_-\\_Last\\_80\\_Years](https://www.researchgate.net/publication/304079106_Active_Noise_Control_From_Analog_to_Digital_-_Last_80_Years), visited 24 October 2020.
- [14] B. Rudzyn and M. Fisher, “Performance of personal active noise reduction devices,” *Applied Acoustics*, vol. 73, pp. 1159–1167, 11 2012.
- [15] X. Qiu, J. Lu, and J. Pan, “A new era for applications of active noise control,” 2014.
- [16] K. Mazur, S. Wrona, and M. Pawelczyk, “Active noise control for a washing machine,” *Applied Acoustics*, vol. 146, pp. 89 – 95, 2019. [Online]. Available: <http://www.sciencedirect.com/science/article/pii/S0003682X18306170>
- [17] A. Kundu and A. Berry, “Active control of transmission loss with smart foams,” *The Journal of the Acoustical Society of America*, vol. 129, pp. 726–40, 02 2011.
- [18] *APx52x B Series AUDIO ANALYZERS*, Audio Precision, 2019, <https://www.ap.com/download/apx52x-series-datasheet-2>, visited 24 October 2020.
- [19] *APx1701 TRANSDUCER TEST INTERFACE*, Audio Precision, 2018, <https://www.ap.com/download/apx1701-datasheet/?wpdmdl=6105>, visited 24 October 2020.
- [20] *GRAS RA0045 externally Polarized Ear Simulator According to IEC 60318-4 (60711)*, GRAS Sound & Vibration A/S, 2018, [https://www.gras.dk/products/ear-simulator/product/ss\\_export/pdf2?product\\_id=248](https://www.gras.dk/products/ear-simulator/product/ss_export/pdf2?product_id=248), visited 24 October 2020.
- [21] G. Ballou et al., *Electroacoustic Devices: Microphones and Loudspeakers*. Focal Press, 2009, vol. 1.
- [22] *Recommendations for Mounting and Connecting InvenSense MEMS Microphones (Application Note AN-1003)*, InvenSense, 2013, <https://3cfeqx1hf82y3xcoull08ihx-wpengine.netdna-ssl.com/wp-content/uploads/2015/02/Recommendations-for-Mounting-and-Connecting-InvenSense-MEMS-Microphones.pdf>, visited 24 October 2020.
- [23] J. Lewis and B. Moss, *MEMS Microphones, the Future for Hearing Aids*, Analog Devices, 2013, <https://www.analog.com/media/en/analog-dialogue/volume-47/number-4/articles/mems-microphones-future-for-hearing-aids.pdf>, visited 24 October 2020.
- [24] H. Zumbahlen, *Phase Relations in Active Filters*, Analog Devices, 2007, <https://www.analog.com/media/en/analog-dialogue/volume-41/number-4/articles/phase-relations-in-active-filters.pdf>, visited 24 October 2020.
- [25] D. Rowell, “2.161 signal processing: Continuous and discrete.” Fall 2008, Massachusetts Institute of Technology: MIT OpenCourseWare, <https://ocw.mit.edu/>. License: Creative Commons BY-NC-SA.
- [26] S. M. Kuo and D. R. Morgan, “Active noise control: a tutorial review,” *Proceedings of the IEEE*, vol. 87, no. 6, pp. 943–973, 1999.
- [27] S. Elliott, *Signal Processing for Active Control*. Academic Press, 2001.

- [28] *Qualcomm® QCC5100 Series Bluetooth Audio SoCs*, Qualcomm, 2020, <https://www.qualcomm.com/media/documents/files/qcc5100-series-product-brief.pdf>, visited 24 October 2020.
- [29] *The State of Play Report 2020*, Qualcomm, 2020, <https://assets.qualcomm.com/the-state-of-play-2020.html>, visited 24 October 2020.
- [30] *LM48560 Boomer™ Audio Power Amplifier Series High Voltage Class H Ceramic Speaker Driver With Automatic Level Control*, Texas Instruments, 2015, <https://www.ti.com/lit/gpn/lm48560>, visited 24 October 2020.
- [31] *SPH1642HT5H-1 HARDY V2 - WIDE BANDWIDTH, LOW NOISE, PRECISION TOP PORT SISONIC™ MICROPHONE*, Knowles Electronics, 2020, [https://www.knowles.com/docs/default-source/default-document-library/sph1642ht5h-1-revf\\_hardy.pdf?Status=Master&sfvrsn=f63971b1\\_0](https://www.knowles.com/docs/default-source/default-document-library/sph1642ht5h-1-revf_hardy.pdf?Status=Master&sfvrsn=f63971b1_0), visited 24 October 2020.
- [32] H. Gether, *Designing a feedback ANC headset using AS3435*, 2015, <https://www.edn.com/design/consumer/4438751/Designing-a-feedback-ANC-headset-using-AS3435>, visited 24 October 2020.
- [33] *MO034402-3 Omnidirectional Electret Condenser Microphone*, DB Unlimited, 2013, [https://www.dbunlimitedco.com/images/product\\_images/2D-Drawings/MO034402-3.pdf](https://www.dbunlimitedco.com/images/product_images/2D-Drawings/MO034402-3.pdf), visited 24 October 2020.
- [34] *ICS-40619 High Dynamic Range Microphone with Differential Output and Low Power*, TDK Corporation, 2016, [https://product.tdk.com/info/en/documents/catalog\\_datasheet/mems-mic/ICS-40619-Datasheet.pdf](https://product.tdk.com/info/en/documents/catalog_datasheet/mems-mic/ICS-40619-Datasheet.pdf), visited 24 October 2020.
- [35] *INMP510 RF-Hardened, Ultra-Low Noise Microphone with Bottom Port and Analog Output*, TDK Corporation, 2014, <https://invensense.tdk.com/wp-content/uploads/2015/02/INMP510.pdf>, visited 24 October 2020.
- [36] *EM288Z1 Specification*, Primo Microphones INC, 2016, specification No. 2C-9246, Release No. 2.
- [37] H. Gether, *Design an ANC headset using the AS3415*, 2014, <https://www.edn.com/design/consumer/4429817/Design-an-ANC-headset-using-the-AS3415>, visited 24 October 2020.
- [38] *AS3460 Digital Augmented Hearing Companion*, ams AG, 2020, [https://www.mouser.cn/pdfDocs/AS3460\\_DS000510\\_NDA\\_1-01.pdf](https://www.mouser.cn/pdfDocs/AS3460_DS000510_NDA_1-01.pdf), visited 24 October 2020.